HHS Public Access

Author manuscript

Nat Cardiovasc Res. Author manuscript; available in PMC 2024 February 15.

Published in final edited form as:

Nat Cardiovasc Res. 2024 January ; 3(1): 60–75. doi:10.1038/s44161-023-00405-9.

Suppression of IL-1β promotes beneficial accumulation of fibroblast-like cells in atherosclerotic plaques in clonal hematopoiesis

Trevor P. Fidler[1,2,3], **Andrew Dunbar**[4,5], **Eunyoung Kim**[6], **Brian Hardaway**[1], **Jessica Pauli**[7,8], **Chenyi Xue**[7], **Sandra Abramowicz**[1], **Tong Xiao**[1], **Kavi O'Connor**[4,5], **Nadja Sachs**[7,8], **Nan Wang**[1], **Lars Maegdefessel**[7,8,9], **Ross Levine**[4,5], **Muredach Reilly**[6,10], **Alan R. Tall**[1]

[1]Division of Molecular Medicine, Department of Medicine, Columbia University Irving Medical Center, New York, NY, USA.

[2]Cardiovascular Research Institute, University of California San Francisco, San Francisco, CA, USA.

[3]Department of Physiology, University of San Francisco, San Francisco, CA, USA.

[4]Human Oncology and Pathogenesis Program, Memorial Sloan Kettering Cancer Center, New York, NY, USA.

[5]Center for Hematologic Malignancies, Memorial Sloan Kettering Cancer Center, New York, NY, USA.

[6]Division of Cardiology, Department of Medicine, Columbia University Irving Medical Center, New York, NY, USA.

[7]Department of Vascular and Endovascular Surgery, Technical University Munich, Munich, Germany.

[8]German Center for Cardiovascular Research (DZHK), Munich, Germany.

Correspondence and requests for materials should be addressed to Trevor P. Fidler or Alan R. Tall. Trevor.Fidler@ucsf.edu; Art1@cumc.columbia.edu.

Author contributions

T.P.F. designed and performed experiments, analyzed data and wrote the manuscript. E.K. and C.X. aided in the design of scRNA-seq studies and conducted scRNA-seq analysis. B.H. designed experiments and aided in mouse studies, immunohistochemistry and analysis of data. A.D. and K.O. aided in studies related to *Dre-Jak2*^{VF}. S.A. and T.X. aided in atherosclerosis studies, processed tissue, and conducted histology experiments and analysis. N.W. designed and performed experiments and analyzed data. L.M., N.S. and J.P. conducted studies of human carotid arteries. R.L. provided reagents and designed experiments. M.R. designed experiments and aided in analysis. A.R.T. designed experiments, analyzed data and wrote the manuscript.

Reporting summary

Further information on research design is available in the Nature Portfolio Reporting Summary linked to this article.

Code availability

No custom code was used in these analyses. All software packages used for data analysis are indicated in the Methods section.

Competing interests

The remaining authors declare no competing interests.

Additional information

Extended data is available for this paper at https://doi.org/10.1038/s44161-023-00405-9.

Supplementary information The online version contains supplementary material available at https://doi.org/10.1038/s44161-023-00405-9.

[9]Department of Medicine, Karolinska Institute, Stockholm, Sweden.

[10]Irving Institute for Clinical and Translational Research, Columbia University Irving Medical Center, New York, NY, USA.

Abstract

Clonal hematopoiesis (CH) is an independent risk factor for atherosclerotic cardiovascular disease. Murine models of CH suggest a central role of inflammasomes and IL-1β in accelerated atherosclerosis and plaque destabilization. Here we show using single-cell RNA sequencing in human carotid plaques that inflammasome components are enriched in macrophages, while the receptor for IL-1β is enriched in fibroblasts and smooth muscle cells (SMCs). To address the role of inflammatory crosstalk in features of plaque destabilization, we conducted SMC fate mapping in *Ldlr*$^{-/-}$ mice modeling *Jak2*^{VF} or *Tet2* CH treated with IL-1β antibodies. Unexpectedly, this treatment minimally affected SMC differentiation, leading instead to a prominent expansion of fibroblast-like cells. Depletion of fibroblasts from mice treated with IL-1β antibody resulted in thinner fibrous caps. Conversely, genetic inactivation of *Jak2*^{VF} during plaque regression promoted fibroblast accumulation and fibrous cap thickening. Our studies suggest that suppression of inflammasomes promotes plaque stabilization by recruiting fibroblast-like cells to the fibrous cap.

Atherosclerotic cardiovascular disease (CVD) is the major cause of death and a principal contributor to disability worldwide[1]. Atherosclerosis arises from the deposition of cholesterol-rich lipoproteins in arteries leading to a macrophage-dominated inflammatory process. Clinical events such as acute coronary syndromes or thrombotic stroke are associated with vulnerable atherosclerotic plaques containing large, lipid-rich necrotic cores and thin fibrous caps[2]. Vascular SMCs also have a prominent role in plaque development and can give rise to a variety of cell types that may have either adverse or beneficial roles in plaque development, including a potential beneficial role in fibrous cap formation[3,4]. In the Canakinumab Anti-inflammatory Thrombosis Outcomes Study (CANTOS), inhibition of IL-1β resulted in a reduction in atherosclerotic CVD[5], especially in patients with *TET2* CH[6]. Similarly, anti-inflammatory treatment with colchicine in the Colcot[7] and LoDoCo trials[8] also reduced CVD. However, the mechanisms underlying the benefit of inflammasome or IL-1β inhibition and the potential links of anti-inflammatory treatments to plaque stabilization remain poorly understood.

CH arises from somatic mutations that provide a fitness advantage to hematopoietic stem cells and leads to the outgrowth of clones of blood cells. CH commonly involves variants in hematopoietic genes that lead to epigenetic modifications (such as *TET2*, *DNMT3A* or *ASXL1*) or increased cytokine signaling (*JAK2*^{VF}). The JAK2 V617F mutation leads to a gain of function in JAK2 which increases hematopoietic cytokine signaling and is commonly found in myeloproliferative neoplasms[9]. The JAK2^{VF} CH variant, although less common than some others, arises at an earlier age[10] and confers the greatest risk of CVD, including premature myocardial infarction[11]. We showed increased atherosclerosis and prominent necrotic core formation in *Ldlr*$^{-/-}$ mice expressing *Jak2*^{VF} selectively in macrophages and in 20% *Jak2*^{VF} chimeric mice that model CH[12]. Deletion of inflammasome components or inhibition of lL-1β consistently increased fibrous caps in *Jak2*^{VF} mice[12], suggesting

plaque stabilization. These interventions did not affect cap thickness in control mice lacking hematopoietic Jak2^{VF} expression[12], possibly because of a lack of prominent inflammasome activation in Western-type diet (WTD)-fed *Ldlr*$^{-/-}$ mice[13]. Furthermore, patients with *JAK2* CH with high predicted AIM2 expression have elevated CVD risk[14]. *Tet2* CH in mice also resulted in accelerated atherosclerosis involving inflammasome activation and increased lL-1β (ref. 2). Importantly, the mechanisms linking IL-1β antagonism to improved features of plaque stabilization were not revealed in these studies[12] and in general remain poorly understood. Here we have used unbiased, high-resolution single-cell and SMC fate mapping and cellular depletion studies to reveal an unanticipated role of fibroblast-like cells, rather than SMCs or their derivatives, in fibrous cap formation in response to lL-1β antagonism or inflammasome suppression resulting from genetic *Jak2*^{VF} inactivation in CH.

Results

Inflammasomes in human carotid atherosclerotic plaques

To assess a potential role of IL-1β in plaque destabilization, we laser dissected fibrous caps from stable and ruptured human carotid lesions. This revealed increased expression of *IL1B* in the caps of ruptured lesions (Fig. 1a), consistent with a role in plaque rupture. To understand how IL-1β signaling may alter fibrous cap formation, we examined early and advanced human carotid plaque specimens obtained from the same individuals (Fig. 1b). Bulk RNA analysis of advanced plaques displayed a clear induction of inflammasome genes (*NLRP3*, *AIM2*, *CAS1*, *IL1b*) and the primary IL-1 signaling receptor *IL1R1* (Fig. 1c), suggesting that IL-1β production and signaling positively associate with lesion progression. Single-cell RNA sequencing (scRNA-seq) of human advanced carotid plaques indicated that monocytes and macrophages displayed the highest expression of inflammasome components while *IL1R1* was primarily expressed in endothelial cells, fibroblasts and SMCs (Fig. 1d,e), suggesting that IL-1β is produced in monocytes and macrophages and subsequently signals to endothelial cells, fibroblasts and SMCs.

IL-1β inhibition promotes accumulation of fibroblasts in the caps of plaques

Human genome-wide association studies have uncovered associations of single nucleotide polymorphisms in a variety of SMC and matrix-related genes with coronary artery disease, suggesting a major role of plaque SMCs or other stromal cell types in plaque stability[15]. Fate mapping and scRNA-seq approaches have revealed transformation of SMCs into a variety of different cell types in advanced atherosclerosis[16], including fibromyocytes that may contribute to plaque stabilization[3]. To assess the hypothesis that IL-1β inhibition would lead to an increase in SMC-derived cells populating the fibrous cap of atherosclerotic lesions, we utilized Myh11-Cre-driven ZsGreen1 reporter mice[17] in mouse models of large variant allele fraction *Jak2*^{VF} and *Tet2* CH. We transplanted chimeric mixtures of 20% *Mx1-Cre*-driven *Jak2*^{V617F} expression (*Mx1*$^{+}$*Jak2*^{VF}) bone marrow with 80% wild-type (WT) CD45.1 bone marrow into irradiated male *Ldlr*$^{-/-}$*Myh11*$^{+}$*ZsGreen1*$^{+}$ mice, which were then pulsed with tamoxifen to induce Myh11-Cre expression and subsequently subjected to a 17-week WTD to induce hypercholesteremia. Antibodies to IL-1β or isotype-matched IgG control were administered for the final 7 weeks of feeding (Fig. 2a). Mice treated with IL-1β antibodies did not display altered mutant burden in blood, plasma cholesterol,

lesion area or necrotic core formation (Extended Data Fig. 1a–f and Supplementary Fig. 1a,b). This is consistent with findings in humans indicating that IL-1β inhibition does not alter plaque size[18]. Similar to female mice modeling *Jak2* CH[12], administration of IL-1β antibodies to male mice with established atherosclerosis led to an increase in fibrous cap thickness (Fig. 2b,c). Histological examination of lesions showed that Zsgreen1^{+}ACTA2^{+} cells were not increased, and in fact overall Zsgreen1^{+} cells were decreased, by IL-1β antagonism (Fig. 2d–i), which is consistent with earlier findings[19]. To profile immune and stromal cells and determine their cellular origin, we conducted scRNA-seq of aortas on flow-separated ZsGreen1^{+} or ZsGreen^{Neg} cells from mice that had been treated with IL-1β or isotype control antibodies (Fig. 2a). We identified 18 unique populations primarily composed of SMCs, fibroblast-like cells and macrophages (Fig. 2j, Extended Data Fig. 1g, Supplementary Fig. 1c and Supplementary Table 1). Surprisingly, IL-1β antagonism only modestly modified the population distribution of SMC-derived cells (ZsGreen1^{+}) (Fig. 2k), with a minor expansion of cluster 5 SMCs (16% to 24%) which had features of contractile SMCs primarily enriched for *Acta2*, *Myh11* and *Tagln* expression and lacking enrichment for matrix proteins.

We also examined ZsGreen1^{Neg} cells, which did not originate from SMCs. Administration of IL-1β antibodies led to a decrease in Zsgreen1^{Neg} macrophages, similar to our previous findings[12], and resulted in a twofold increase in cluster 6 fibroblast-like cells (from 9% to 20%) (Fig. 2i). Cluster 1 fibroblasts were also increased but more moderately (from 18% to 20%). These cells did not have prominent expression of fibroblast activation protein (*Fap*), which may be increased by IL-1β signaling and contribute to the progression of heart failure[20,21], but rather were primarily enriched for transcripts related to matrix production, *Col1a1*, *Col1a2*, *Dcn* and *Lum* (Fig. 3 and Supplementary Table 1), suggesting a potential role in repair mechanisms promoting fibrous cap formation in response to IL-1β antibody therapy. Stratifying cells based on ZsGreen1 and IL-1β antibody status revealed that *Dcn* was highly enriched in ZsGreen1^{Neg} cells, specifically in fibroblast-like cells (Fig. 4a,b). Histological examination in proximal aortas confirmed a significant IL-1β antibody-mediated increase in Decorin protein expression in the intima of lesions (Fig. 4c,d), consistent with an expansion of fibroblast-like cells. Moreover, this increase in fibroblasts was most prominent in the fibrous cap (Fig. 4c,e).

We next conducted studies to assess potential mechanisms of accumulation of fibroblasts in the cap region following IL-1β inhibition. The transcriptional signature of cluster 6 fibroblast-like cells partially resembled mesenchymal stem cell (MSC)-derived cardiac fibroblasts[22]. To determine if inhibition of IL-1 signaling would increase recruitment of adventitial MSC-derived fibroblasts in *Jak2*^{VF} CH, we selectively deleted *Il1r1* from MSCs using *Gli1-Cre* (ref. 23). However, *Il1r1* deficiency in MSCs did not lead to alteration of cap formation in WTD-fed *Jak2*^{VF} CH mice (Extended Data Fig. 2a,b). Consistently, ZsGreen1 labeling of MSC-derived cells indicated predominant accumulation in the adventitia and valves (magenta cells in Extended Data Fig. 2c,d), with only rare cells labeled in the cap region (arrows in Extended Data Fig. 2c) and no overall increase in ZsGreen1^{+} cells in lesions with IL1R1 deficiency in MSCs (Extended Data Fig. 2d). Since cap fibroblasts were not increased when IL1R1 was ablated in MSCs, we further examined scRNA-seq data for differentially expressed genes in fibroblasts with respect to IL-1β status. Gene

ontology enrichment analysis of cluster 1 and 6 fibroblasts in *Jak2*^{VF} CH mice showed top terms related to extracellular structure, extracellular matrix organization, cell motility and migration for cluster 1 fibroblasts, while cluster 6 fibroblasts showed top terms related to protein synthesis and mitochondrial respiratory chain activity, suggesting metabolically active cells (Supplementary Tables 1 and 2). The cell migration gene *Tmsb10* (ref. 24) was one of the top ten genes differentially expressed by cluster 6 fibroblasts (Supplementary Table 1), suggesting that IL-1β antagonism may promote fibroblast accumulation through enhanced migration to the cap of fibroblasts that are already resident in the vessel, possibly from the adventitia where there was prominent Decorin staining (Fig. 4c).

Since myeloid cell *Tet2* deficiency in a mouse model of CH has been shown to promote IL-1β expression and inflammasome activation[2], we also examined a potential role of fibroblasts in response to IL-1β inhibition in *Tet2* CH by transplanting 20% bone marrow with monocyte/macrophage restricted deletion of *Tet2* (Cx3cr1-*Tet2*$^{fl/fl}$) with 80% CD45.1 bone marrow into *Ldlr*$^{-/-}$*Myh11*$^{+}$*ZsGreen1*$^{+}$ reporter mice. The mice were then subjected to a similar experimental protocol as *Jak2* CH mice (Fig. 2a). Administration of IL-1β antibodies resulted in a ~5% increase in Tet2 burden in blood and did not alter lesion area or necrotic core formation (Extended Data Fig. 3a–e). Similar to the *Jak2*^{VF} CH mice, IL-1β antibody treatment did not alter Zsgreen1^{+} SMCs or their progeny, with only an expansion of a minor SMC population (cluster 13) (8.2% to 12%) with contractile features shown by enrichment for *Acta2*, *Myh11* and *Tagln* (Fig. 5a–c, Extended Data Fig. 3f and Supplementary Table 3). However, ZsGreen1^{Neg} cells showed a large increase in the major population (cluster 0, from 14% to 20%) of fibroblast-like cells, a smaller increase in cluster 6 fibroblasts (from 3% to 6%), as well as a reduction in monocytes and neutrophils. The fibroblast-like cells lacked *Fap* expression (except for cluster 8) and were enriched for *Col1a1*, *Col1a2*, *Dcn* and *Lum* (Fig. 5d–h and Supplementary Table 3). Gene ontology analysis for cluster 0 fibroblasts showed top terms related to extracellular structure, extracellular matrix organization, cell motility and migration (Supplementary Table 4), resembling the cluster 1 fibroblasts that were increased by IL-1β antibodies in *Jak2*^{VF} CH mice, while cluster 6 fibroblasts were enriched for terms related to mitochondrial electron transport chain and synthetic processes, similar to the cluster 6 fibroblasts from the *Jak2*^{VF} mice (Supplementary Table 4). Our previous work in female mice indicated that IL-1β inhibition only benefited features of plaques stability in mice with prominent inflammasome activation[12]. Consistent with these earlier findings, administration of IL-1β antibodies to WTD-fed male *Ldlr*$^{-/-}$ mice with WT bone marrow did not result in changes in fibroblast-like cell accumulation or SMC differentiation (Extended Data Fig. 4). Thus, in two different models of CH which have activation of inflammasomes, but not in standard *Ldlr*$^{-/-}$ mice, IL-1β inhibition promotes the accumulation of distinct populations of non-SMC-derived fibroblast-like cells within atheromas, providing insight into the mechanism of fibrous cap formation and plaque stabilization in response to IL-1β antibody treatment.

IL-1β antagonism promotes cap thickening through *Prg4*$^{+}$ cells

To further define the role of fibroblast-like cells in fibrous cap formation, we next attempted to remove these cells from lesions using a targeted diphtheria toxin approach. scRNA-seq analysis of *Jak2* and *Tet2* lesions revealed that fibroblast-like cells from aortas were enriched

for proteoglycan genes (*Dcn* and *Lum*). Recent scRNA-seq of murine atheromas revealed that the proteoglycan *Prg4* is enriched in plaque stromal cells, including modulated SMCs and non-SMC-derived fibroblasts[3]. Examination of *Prg4* in scRNA-seq data of aortas revealed that *Prg4* expression was enriched in fibroblast-like cell populations with modest expression in SMC-derived intermediate SEM cells (stem cell, endothelial cell, monocyte-like cells) from *Jak2* and *Tet2* CH mice (Fig. 6a–c and Extended Data Fig. 5a–e). RNAscope analysis revealed that *Prg4*$^{+}$ cells in atheromas increased in *Jak2* CH mice treated with the IL-1 receptor antagonist anakinra (Fig. 6d,e), consistent with the scRNA-seq data.

To selectively ablate *Prg4*$^{+}$ cells, we generated *Ldlr*$^{-/-}$ mice with or without *Prg4*-Cre (ref. 25)-driven diphtheria toxin A expression (*Ldlr*$^{-/-}$*Prg4-Cre*$^{+}$ or *Ldlr*$^{-/-}$*Prg4-Cre*$^{+}$*iDTA*$^{+}$). We then transplanted 20% *Jak2*^{VF} bone marrow into these mice to model CH and subjected these mice to a WTD for 14 weeks; IL-1β antibodies, diphtheria toxin and tamoxifen were administrated during the last 4 weeks of feeding (Fig. 6f). Depletion of *Prg4*$^{+}$ cells did not alter lesion area or necrotic core area (Fig. 6g–i). However, depletion of *Prg4*$^{+}$ cells led to a significant reduction in cap thickness (Fig. 6j,k), confirming that *Prg4*-expressing cells, likely including fibroblast-like cells, promote fibrous cap thickening during IL-1β antibody treatment. *Ldlr*$^{-/-}$ mice transplanted with WT bone marrow and subjected to a similar *Prg4*$^{+}$ cell depletion and IL-1β antibody protocol did not show altered lesion area or necrotic core area; however, there was a nonsignificant reduction in cap thickness (Extended Data Fig. 5f–j). Thus, in the setting of IL-1β antagonism in *Jak2*^{VF} CH mice, *Prg4*$^{+}$ cells aid in promoting fibrous cap thickening and increasing features of plaque stability.

Selective ablation of *Jak2* V617F mutation promotes fibrous cap formation

In our previous studies, attempts to suppress atherosclerosis with ruxolitinib, which is used to treat *JAK2*^{VF} myeloproliferative neoplasms, led to worsening of features of plaque stability, including thinning of fibrous caps, and subsequent safety monitoring studies led to an Food and Drug Administration warning concerning increased CVD risk associated with broad-spectrum JAK inhibitors[26]. To assess the impact of targeted, more specific inactivation of *Jak2*^{VF} on features of plaque stability, we employed a mouse model in which *Jak2*^{VF} can be selectively inactivated by a genetic approach[27]. *Jak2*^{VF} was expressed ex vivo in bone marrow cells by electroporating DRE Recombinase. The transduced bone marrow was mixed with CD45.1^{+} WT bone marrow (20%:80%, respectively) and then transplanted into *Ldlr*$^{-/-}$ mice to model CH. After atherosclerosis was established, *Jak2* mutant exons were excised by Cre-mediated recombination of flanking lox p sites using tamoxifen induction of Ubc^{ERT}Cre (Fig. 7a). Mice harboring Dre-induced *Jak2*^{VF} expression had increased blood leukocyte counts as well as increased monocytes which were significantly reduced following tamoxifen administration in conjunction with a reduction in spleen weight (Extended Data Fig. 6), indicating a correction of hematological disease similar to findings in chow-fed mice[27]. scRNA-seq analysis of CD45^{+} cells from aortas revealed substantial changes in immune cell distribution, including a major expansion of CD8 T cells (clusters 0, 1 and 2), in mice with *Jak2*^{VF} turned off (*Jak2*^{VF} Off) (Extended Data Fig. 7a–c). Stratification of cell types based on CD45.1 (WT) or CD45.2 in *Jak2*^{VF} or littermate control mice using cellular indexing of transcriptomes and epitopes (CITE-seq) revealed that *Jak2*^{VF} Off lesions were almost devoid of CD45.2^{+} mutant cells (Extended Data Fig.

7d–g), suggesting an inability of mutant myeloid cells to compensate for the loss of the *Jak2*^{VF} mutation. However, the larger lesion size in *Jak2*^{VF} compared with control mice was not reversed by turning off *Jak2*^{VF} (Extended Data Fig. 8a,b), and features of plaque stability, percentage necrotic core area, cap thickness, Decorin expression, collagen content and macrophage density (Extended Data Fig. 8c–j) were not improved. Humans and mice carrying the *Jak2*^{VF} mutation have decreased cholesterol levels, yet their coronary artery disease risk remains high[28]. Turning off *Jak2*^{VF} during plaque regression led to a marked increase in plasma cholesterol (Extended Data Fig. 8k), potentially explaining the lack of improvement in plaques.

In a further attempt to improve features of plaque stabilization, we next inactivated *Jak2*^{VF} in conjunction with effective cholesterol lowering, simulating a potential therapeutic scenario where JAK2^{VF}-specific inactivation would occur in combination with treatment with statins or other Cholesterol-lowering agents. We transplanted *Ldlr*$^{-/-}$ mice with 20% bone marrow from mice with Dre-induced *Jak2*^{VF} expression with or without Ubc^{ERT}-Cre and 80% WT bone marrow. Mice were allowed to establish lesions by WTD feeding for 12 weeks. *Jak2*^{VF} was then turned off, and *LDLR* adenovirus was administered to restore *LDLR* expression in conjunction with low-cholesterol diet feeding (Fig. 7b). Serum cholesterol levels decreased to a similar extent in mice with continuous *Jak2*^{VF} expression (*Jak2*^{VF} On) or with *Jak2*^{VF} turned off (Fig. 7c). Turning off *Jak2*^{VF} significantly reduced serum IL-1β concentrations (Fig. 7d). Lowering cholesterol levels led to no change in lesion area or percentage necrotic core area (Fig. 7e–g). However, we found that mice with *Jak2*^{VF} Off had significantly increased cap thickness and collagen content (Fig. 8a–c) and increased expression of Decorin in lesions (Fig. 8d,e), suggesting that turning off *Jak2*^{VF} promotes fibroblast-like cell accumulation in lesions and increases cap thickness. Cholesterol lowering in *Jak2*^{VF} On mice produced a significant reduction in overall macrophage burden, a consistent finding during atherosclerotic plaque regression (Fig. 8f,g)[29]. Unexpectedly, this reduction in macrophages appeared blunted when *Jak2*^{VF} was turned off. To understand this, we performed scRNA-seq analysis focused on CD45^{+} immune cells in plaques. Similar to Dre-*Jak2*^{VF} mice without cholesterol lowering, turning *Jak2*^{VF} Off led to an expansion of cluster 0 CD8 T cells (Extended Data Fig. 8a–c), which had surface expression of CD134, CD137, CD1d, Ly108 and CD155 as indicated by CITE-seq (Supplementary Fig. 2). To understand the changes in macrophages, we re-clustered scRNA-seq data to focus on myeloid cell populations (Fig. 8h and Extended Data Fig. 9d). This showed a prominent expansion of Trem2-high and Lyve-1^{+} resident-like macrophages (Fig. 8i). In plaque progression studies[30], Trem2-high macrophages are noninflammatory, while in other disease settings Trem2-high macrophages secrete fibrogenic factors[31], potentially linking them to increased fibrous cap formation. Thus, combined cholesterol lowering and *Jak2*^{VF} inactivation reduced IL-1β and produced features of plaque stabilization, including an increase in fibroblasts and fibrous cap formation as well as an increase in noninflammatory, potentially fibrogenic (*Spp1* and *Col14a1* enriched) Trem2^{Hi} macrophages.

Discussion

Atherosclerotic plaque rupture and erosion are inciting events of myocardial infarction and stroke. Plaque imaging studies have recently shown that interventions that were beneficial

in human clinical outcome trials (PCSK9 antibodies added to statins) led to a marked increase in fibrous cap thickness compared with placebo-treated control subjects[32,33], which along with studies of human carotid plaques[2,34] suggest the key importance of increased fibrous cap thickening in plaque stabilization and improved clinical outcomes. While mice do not reliably rupture atherosclerotic plaques, major determinants of plaque vulnerability, such as fibrous cap thickness and necrotic core formation, can be investigated and underlying mechanisms can be probed by use of genetic and therapeutic interventions combined with high-resolution single-cell and cell fate mapping studies. Our study shows that inflammasome suppression or IL-1β inhibition in mouse models of CH with prominent plaque inflammation and inflammasome activation leads to an increase in fibrous cap formation, suggesting plaque stabilization. Surprisingly, in two different models of CH, IL-1β antagonism was associated with an increase in non-SMC-derived fibroblast-like cells. Previous studies have suggested an important role of SMCs in fibrous cap formation during plaque progression[3,4]. However, these studies were not performed in the context of anti-inflammatory treatment by inflammasome or IL-1β inhibition. Thus, our studies reveal a role of fibroblasts in therapeutic plaque reparative processes increasing fibrous cap formation and stabilizing plaques during inflammation suppression.

Similar to vascular SMCs, fibroblasts are cells with high plasticity that can assume a variety of different phenotypes in homeostasis or disease settings. Commonly, activated fibroblast states are associated with a worsening of outcomes, such as in heart failure[35] and rheumatoid arthritis[36]. Accordingly, targeting fibroblast activation with specific inhibitors, IL-1β antagonism or activated fibroblast cell depletion therapies[20,21,37] have emerged as potential treatments for heart failure. A recent study has shown exacerbation of cardiac fibrosis and heart failure in DNMT3A CH mice related to macrophage–fibroblast crosstalk[38]. Our findings suggest that distinct types of noninflammatory fibroblasts were increased in *Jak2*^{VF} and *Tet2* CH mice by IL-1β inhibition. Cellular localization and depletion studies provided evidence that depletion of fibroblast-like cells prevented cap thickening in response to IL-1β inhibition. Unexpectedly, fate mapping studies indicated that these cells did not originate from MSCs but rather were likely derived by migration or proliferation of resident fibroblasts. Interestingly, scRNA-seq analysis suggested that two distinct types of fibroblasts were increased by IL-1β inhibition: one with high expression of matrix-forming and cell migration genes and another with increased expression of mitochondrial electron transport chain and synthetic genes, suggesting high metabolic activity. Further studies will be required to define the roles of different types of fibroblasts in fibrous cap stabilization.

Our studies using human carotid artery atherectomy specimens provide evidence for a role of inflammasomes in more advanced plaques and specifically associate high expression of *IL1b* in the cap with plaque rupture. Our studies in mice with inflammatory plaques show that IL-1β inhibition consistently increases fibrous cap thickness, together suggesting that this may be a key mechanism to explain the benefit of anti-inflammatory treatments in humans. While CANTOS[5] and colchicine[8] anti-inflammatory treatments produced CVD benefit, this has not yet led to widespread adoption of these treatments for CVD. Studies in mouse models and a subset analysis of CANTOS have suggested that these treatments should be precisely targeted to the most at-risk patients, such as those with CH[6]. This

concept is reinforced by our study revealing a mechanism-based benefit of targeted inflammasome or IL-1β suppression in the setting of CH.

Our studies have several limitations. Although human subjects were elderly, they were not specifically genotyped for CH mutations. Because in our previous mouse work we did not find an impact of IL-1β inhibition on cap thickness in control *Ldlr*$^{-/-}$ mice, we included this group only in representative experiments in the current studies where IL-1β inhibition had no or lesser impact on plaque morphology and fibroblast populations. Similar to our findings others have reported a decrease in ACTA2^{+} SMCs in plaques after IL-1β inhibition[19]; however, dissimilar to our work this was associated with a decrease in collagen staining in the fibrous cap[19]. This could be related to differences in the mouse strain, stage of lesions, site of atherosclerosis or other factors; however, the most salient difference is that we employed models of aggravated plaque inflammasome activation due to CH mutations. In our studies we employed a high allele burden model (20% variant allele fraction) which may not be informative for lower allele burden CH. Finally, the translational impact of our work remains largely speculative as patients are not routinely genotyped for CH mutations, and the ultimate risk/benefit ratio of anti-inflammatory interventions in patients with CH will require focused clinical trials.

Methods

Inclusion and ethics

All research reported here complies with all relevant ethical regulations. Human carotid artery samples were collected from the Munich Vascular Biobank upon patients' informed consent. The Munich Vascular Biobank is approved by the local Hospital Ethics Committee (2799/10, Ethikkommission der Fakultat fur Medizin der Technischen Universitat Munchen, Munich, Germany) and in accordance with the Declaration of Helsinki. Subjects were not compensated. All animal studies were performed in accordance with institutional guidelines in accordance with Institutional Animal Care and Use Committee of Columbia University and those established by Memorial Sloan Kettering Cancer Center (MSKCC) under the Institutional Animal Care and Use Committee-approved animal protocol (no. 07–10-016) and the Guide for the Care and Use of Laboratory Animals (National Academy of Sciences 1996).

Human carotid artery analysis

Human carotid artery samples were collected from the Munich Vascular Biobank upon patients' informed consent and stored in RNAlater directly after surgical removal, after which they were cut into several pieces and further processed for molecular analyses[39]. Patient characteristics are summarized in Supplementary Table 5.

Bulk-cell RNA sequencing.—Human carotid arteries (advanced plaque versus early lesion from the same individual patient) were cut on dry ice into pieces of ~50 mg each. Tissue was homogenized in 700 μl of Qiazol lysis reagent and total RNA was isolated using the miRNeasy Mini Kit (Qiagen) according to the manufacturer's protocol. RNA quantity was fluorometrically assessed using Qubit 3 (Thermo Fisher). RNA Integrity Number was

assessed using RNA Screen Tape (Agilent) utilizing Agilent TapeStation 4200. Extracted total RNA from 37 patients (74 samples, 2 samples per patient) was purified using poly-T oligo-attached magnetic beads. The library was prepared using TruSeq stranded messenger RNA kit (Illumina), following the manufacturer's instructions, and sequenced using the Illumina NovaSeq platform, 35–40 million reads per sample (NovaSeq6000, Illumina). RNA raw data (raw reads) of FASTQ format were analyzed by Fios Genomics. Quality control was performed on the raw FASTQ files as well as the alignment statistics generated by the STAR aligner during the data processing protocol. All samples exhibited high quality and consistent sequence length distributions, and were all included in subsequent analyses (Fios Genomics).

scRNA-seq.—Human carotid arteries were collected during carotid endarterectomy in the Department of Vascular and Endovascular Surgery (Klinikum rechts der Isar, Technical University Munich) and stored directly on ice in PBS. Tissues were minced and digested using the Multi Tissue Dissociation Kit 2 (Miltenyi Biotech, 130–110-203), GentleMACS Dissociator (Miltenyi Biotech, 649 130–093-235), GentleMACS C tubes (Miltenyi Biotech, 130–096-334) and the 37C_Mulit_G 650 program, all according to the manufacturer's instructions. The cell suspension was strained (70 μm, 40 μm) and Dead Cell Removal (Miltenyi Biotech, 130–090-101) using MS Columns (Miltenyi Biotech, 130–042-201) was performed. Cells were resuspended in PBS + 0.04% BSA. Only cell suspensions that were clean enough were used for further single-cell capture.

Cells were loaded into a 10x Genomics microfluidics Chip G and encapsulated with barcoded oligo-dT-containing gel beads using the 10x Genomics Chromium Controller. Gel beads-in-emulsion clean-up, complementary DNA amplification and 3′ Gene Expression Library construction were performed according to the manufacturer's instructions (CG000204 Rev D). Quantity and purity of cDNA and final libraries were assessed using Qubit 3 (Thermo Fisher) and Agilent TapeStation 4200 (Agilent). Libraries from individual samples were multiplexed into one lane before sequencing on an Illumina NovaSeq6000 instrument.

For scRNA-seq analysis, the R package Seurat (v.4.1.1) was utilized in RStudio (v.1.4.1717)[4]. Genes were eliminated from downstream analysis if they were expressed in fewer than five cells, and cells with maximum mitochondrial reads >15%, maximum unique molecular identifiers (UMIs) greater than 20,000, minimum genes less than 100 and maximum genes greater than 4,000 were filtered out in each Seurat object. After quality control, 6,108 cells were included for downstream analysis.

Laser capture micro-dissection of stable and unstable carotid artery plaques.—Carotid atherosclerotic lesions from the Munich Vascular Biobank were paraffin-embedded, sectioned and then stained with hematoxylin and eosin (H&E) on RNase-free glass slides as briefly described below. Sections were pretreated with ultraviolet light (254 nm) for 30 min to enhance adhesion of the paraffin-embedded tissue specimens. Laser capture micro-dissection of advanced atherosclerotic lesions (either stable or unstable; n = 10 versus 10) was performed as previously described[40,41]. The Taqman High-Capacity cDNA Transcription Kit (Thermo Fisher) was used for cDNA synthesis, and primer

assays for *IL1B* (assay ID: Hs01555410_m1) and *GAPDH* (assay ID: Hs02786624_g1) (endogenous control; both from Thermo Fisher) were used to detect changes in expression levels.

Animals

All experiments utilized bone marrow transplantation (BMT), with donor mice sex-matched to recipients. Donor mice were 6–14 weeks old and recipient mice were 8–12 weeks old. All mice used for these studies were on a C57Bl/6J background and were housed at Columbia University or MSKCC in a dedicated pathogen-free facility under standard conditions of temperature with a 12-h light/dark cycle and food available ad lib. All animal experiments were conducted in accordance with the Institutional Animal Care and Use Committee of Columbia University or MSKCC. *Tet2* floxed mice were obtained from the Jackson Lab (B6;129S-*Tet2*$^{tm1.1Iaai}$/J, 017573) and crossed to mice harboring a *Cx3cr1-Cre* (B6J.B6N(Cg)-*Cx3cr1*$^{tm1.1(cre)Jung}$/J, 025524) from the Jackson Lab. *Jak2V617F* conditional knock-ins have been previously described[42] and were induced with an *Mx1-Cre* (Jackson Lab, B6.Cg-Tg(Mx1-cre)1Cgn/J, no. 003556). *Ldlr*$^{-/-}$*Myh11-ZsGreen1*$^{+}$ reporter mice were previously described[17]. *Prg4-Cre* mice (P*rg4*$^{tm1(GFP/cre/ERT2)Abl}$/J, Jackson Lab no. 022757) were crossed to *Ldlr*$^{-/-}$ mice (B6.129S7-*Ldlr*^{tm1Her}/J, Jackson Lab no. 002207) and mice with Cre-inducible diphtheria toxin A (iDTA) expression (B6.Cg-*Gt(ROSA)26Sor*$^{tm2.1(CAG-EGFP,-DTA*G128D)Pjen}$/J, Jackson Lab no. 026944). Gli1-Cre mice (Gli1$^{tm3(cre/ERT2)Alj}$/J, Jackson Lab no. 007913) were crossed to *Ldlr*$^{-/-}$ mice (B6.129S7-*Ldlr*^{tm1Her}/J, Jackson Lab no. 002207), mice with a Cre-inducible ZsGreen1 reporter (B6.Cg-*Gt(ROSA)26Sor*$^{tm6(CAG-ZsGreen1)Hze}$/J, Jackson Lab no. 007906) and *Il1r1* floxed mice (B6.129(Cg)-*Il1r1*$^{tm1.1Rbl}$/J, Jackson Lab). *Dre-Jak2V617F* mice were generated as previously described[27]. Myh11-Cre studies were conducted only in male mice since this Cre is X-linked. Studies of Prg4-Cre mice utilized both male and female mice. Dre-Jak2 studies were conducted only in female mice to compare with historical studies that utilized Mx-Cre Jak2 mice.

DreCre *Jak2*^{VF} knock-in/knockout mouse studies

Jak2^{VF} knock-in/knockout mice were utilized as previously described[27]. To induce *Jak2*^{VF}, Dre mRNA electroporation ex vivo was performed. Specifically, whole bone marrow donor cells from UbcCreER-*Jak2*^{VF} DreCre mice were isolated from limb bones and single-cell suspensions lysed of red blood cells (RBCs) (ThermoScientific). Bone marrow was then depleted of lineage-committed hematopoietic cells using a lineage cell depletion kit according to the manufacturer's protocol (EasySep, StemCell Technologies) and cultured for 2 h in StemSpan SFEM medium with thrombopoietin (20 ng ml^{-1}; PeproTech) and stem cell factor (20 ng ml^{-1}; PeproTech). Cells were subsequently collected, washed in PBS and resuspended in 135 µl of Electroporation Buffer T (Invitrogen) to which 15 µl of Dre mRNA (at 1 µg µl^{-1}) was quickly added and electroporated at the following conditions: 1,700 V for 20 ms ×1 pulse per the manufacturer's protocol (Invitrogen Neon Transfection System). The cells were then pipetted into penicillin-streptomycin-free StemSpan SFEM medium with thrombopoietin (20 ng ml^{-1}; PeproTech) and stem cell factor (20 ng ml^{-1}; PeproTech) and cultured overnight at 37 °C. Cells were then collected and washed/resuspended in PBS and transplanted via lateral tail vein injection into lethally irradiated (900 cGy) 6–

8-weekold C57BL/6J recipient mice at approximately 4×10^5 cells per recipient along with 50,000 un-electroporated WT whole bone marrow support cells. At 6–8 weeks following electroporation/transplant, UbcCreER*Jak2*^{VF} DreCre recipient mice demonstrating elevated leukocyte counts in blood were then killed and whole bone marrow was collected for secondary transplantation for atherosclerosis studies.

For atherosclerosis progression studies of *Dre-Jak2*^{VF}, 20% bone marrow from CD45.2$^+$ *Dre-Jak2*^{VF} with UBC2^{ERT}-Cre was mixed with 80% WT CD45.1 bone marrow and transplanted into lethally irradiated female *Ldlr*$^{-/-}$ mice. After 4 weeks of recovery, mice were subjected to WTD feeding (ENVIGO, cat. no. TD.88137). For progression studies mice were subjected to 12 weeks of WTD, then control and *Jak2*^{VF} Off mice were fed WTD with tamoxifen at 500 mg kg^{-1} by weight (ENVIGO, cat. no. TD130889) for 1 week then returned to WTD without tamoxifen for 17 more days.

For regression studies 20% bone marrow from CD45.2$^+$*Dre-Jak2*^{VF} mice with a Ubc2^{ERT}-Cre (*Jak2*^{VF} Off) or without Cre (*Jak2*^{VF} On) were mixed with 80% CD45.1 bone marrow and transplanted into lethally irradiated female *Ldlr*$^{-/-}$ mice. Following BMT, all mice expressed Jak2^{VF} under the control of Dre. At 4 weeks post BMT, mice were placed on a WTD for 9 weeks. Mice were then fed a WTD supplemented with 500 mg kg^{-1} tamoxifen for 1 week, then injected intravenously with adenoviruses with human *LDLR* transgene to restore LDLR expression in liver and reduce plasma cholesterol, as previously described[43], and were placed on a chow diet for 50 more days until terminal collection.

BMT

For BMT studies, donor mice were euthanized and bone marrow flushed with HBSS, filtered through a 40-μm cell filter and centrifuged at 800*g* for 10 min. RBCs were then lysed with RBC lysis buffer (Biolegend cat. no. 420302), washed and resuspended in RPMI. Then, 4×10^6 bone marrow cells were intravenously injected into lethally irradiated recipient mice, which were irradiated with 10.5 gly from a cesium source. Mice were allowed to recover for 4 weeks.

Atherosclerosis studies

Atherosclerosis studies were powered for an 80% chance of detecting a >33% change in atherosclerosis lesion size based on 25–30% variation with a $P < 0.05$. Studies were conducted 4 weeks post BMT by treatment with WTD (ENVIGO, cat. no. TD88137) or WTD containing tamoxifen at 0.5 g kg^{-1} by weight (ENVIGO, cat. no. TD130889), as indicated. When using Mx1-Cre, 4 weeks post-BMT mice were injected intraperitoneally with 50 μg per mouse per day of polyinosinic:polycytidylic acid (pIpC) (Sigma P1530), twice with a 1-d interval, then WTD feeding was initiated 1 week later. Isoflurane anesthetized mice were bled serially by cheek puncture for analysis of blood parameters at the indicated timepoints. For terminal collection, mice were perfused with 20 ml of PBS and aortic roots were fixed for 48 h in 4% paraformaldehyde, then embedded in paraffin and sectioned for histological analysis.

Myh11-ZsGreen1 studies.—For SMC reporter experiments, *Myh11-Cre*^{ERT2} (Jackson Lab, cat. no. 019079) mice were crossed with *Ldlr*$^{-/-}$ (Jackson Lab, cat. no. 002207) and *ZsGreen1* (B6.Cg-*Gt(ROSA)26Sor*$^{tm6(CAG-ZsGreen1)Hze}$/J, Jackson Lab, cat. no. 007906) mice to generate *Ldlr*$^{-/-}$*Myh11*$^{+}$*ZsGreen1*$^{+}$ reporter mice, as previously described[17]. For atherosclerosis studies, *Ldlr*$^{-/-}$*Myh11*$^{+}$*ZsGreen1*$^{+}$ reporter mice were lethally irradiated with 10.5 gly and transplanted with 20% bone marrow from CD45.2^{+}*Mx1*$^{+}$*Jak2*^{VF} mice mixed with 80% WT CD45.1^{+} bone marrow to model CH. For *Tet2* studies, 20% CD45.2^{+}*Cx3cr1-Tet2*$^{-/-}$ bone marrow was mixed with 80% CD45.1^{+} WT bone marrow to model CH. For Myh11-Cre expression, 500 mg kg^{-1} tamoxifen-supplemented WTD (ENVIGO, cat. no. TD130889) was administered for 7 d at initiation of WTD feeding as indicated in Fig. 1e. When indicated, IL-1β antibodies (10 mg kg^{-1}) or IgG control (10 mg kg^{-1}) were administered subcutaneously weekly at the indicated timepoints, as previously described[44] and indicated in Fig. 1e.

For *Prg4* cell ablation studies, Prg4-Cre^{ERT2} mice (P*rg4*$^{tm1(GFP/cre/ERT2)Abl}$/J, Jackson Lab no. 022757) were crossed to *Ldlr*$^{-/-}$ mice (B6.129S7-*Ldlr*^{tm1Her}/J, Jackson Lab no. 002207) and mice with iDTA expression (B6.Cg-*Gt(ROSA)26Sor*$^{tm2.1(CAG-EGFP,-DTA*G128D)Pjen}$/J, Jackson Lab no. 026944) to generate *Ldlr*$^{-/-}$*Prg4*$^{+}$*iDTA*$^{+}$ mice. Male and female *Ldlr*$^{-/-}$*Prg4*$^{+}$*iDTA*$^{+}$ mice or littermate *Ldlr*$^{-/-}$*Prg4*$^{+}$ mice were lethally irradiated with 10.5 gly and transplanted with 20% *Mx1*$^{+}$*Jak2*^{VF} or WT bone marrow mixed with 80% WT bone marrow to model CH. Mice were allowed to recover for 4 weeks followed by pIpC injections, and WTD feeding for 10 weeks, as indicated in Fig. 6f. All mice were then injected with IL-1β antibodies (10 mg kg^{-1}) and diphtheria toxin (10 ng per mouse) along with a WTD supplemented with 500 mg kg^{-1} tamoxifen by weight (ENVIGO, cat. no. TD130889) to induce Prg4-Cre and iDTA expression.

Histological analysis

Aortic root lesions were sectioned serially at 6-μm thickness. Sections were stained with H&E (Sigma) and lesion area and necrotic core area were determined in six serial sections 60 μm apart as previously described[13]. Slides were imaged using Nikon Labphoto 2 and Image Pro Plus software (Media Cybernetics v.7.0.0.591) and blinded researchers quantified lesion area and necrotic core area in FIJI software[45].

For cap thickness analysis, slides from similar regions in the aortic root were stained with picrosirius red (Polysciences). Cap thickness was measured as previously described[12]. Caps from the largest lesions per section were quantified at 2-μm intervals, with the average thickness reported.

Immunofluorescence analysis

Immunofluorescence analysis was conducted on paraffin-embedded aortic root sections following deparaffination and citric acid-based antigen retrieval (Vector Laboratories, H3300) with 20 min of heat and pressure. Slides were washed with PBS with 0.1% Tween 20 (PBST) four times and blocked with 10% goat serum (Biolegend cat. no. 927503) for 30 min at room temperature. Primary antibodies were then incubated overnight in 5% goat serum, after which slides were washed with PBST and stained with DAPI (1 ng ml^{-1}) and

secondary Alexa fluor antibodies at 1:1,000 dilution (Thermo Fisher). Slides were washed four more times with PBST and then mounted in ProLong Gold antifade reagent with DAPI (Thermo Fisher, cat. no. P36935). Slides were imaged on a Nikon Ti Eclipse inverted confocal microscope. Images were analyzed with FIJI software.

Macrophage density was determined as lesion area occupied by MAC2 (1:500) staining (Cedarlanes, CL8942AP). ZsGreen1 (1:1,000) antibodies (Thermo Fisher, TA180002) were used to visualize ZsGreen1^{+} cells in lesions. Antibodies for ACTA2 (1:500) (Millipore Sigma, C6198) and Decorin (1:1,000) (Abcam, ab277636) were used for immunofluorescence analysis.

RNAscope

Female *Ldlr*$^{-/-}$ mice modeling *Jak2*^{VF} CH were subjected to a 12-week WTD with 10 mg kg^{-1} anakinra administered 6 d per week intraperitoneally as previously described[12]. The RNAscope Multiplex Fluorescent Reagent Kit v2 process was conducted on paraffin-embedded aortas based on the manufacturer's protocols (ACD Bio, 323100), and sections were stained for Prg4 (MmPrg4, no. 437661) and DAPI.

Serum analysis

Mouse serum was isolated through centrifugation of blood at 12,000*g* for 10 min at 4 °C. Serum was evaluated for IL-1β through ELISA (Abcam, cat. no. ab229440). Serum cholesterol was determined with a Cholesterol E assay (Wako, cat. no. 999–02601).

Blood cell analysis

Blood from mice was collected at the indicated timepoints through cheek bleed into EDTA-coated tubes. Blood cell numbers were then quantified with the VetScan HM5 Hematology system (Abaxis). For flow cytometry analysis, RBCs were lysed with RBC lysis buffer, washed in PBS with 0.5% BSA and 2 mM EDTA, then stained with the indicated antibodies. CD45.1/2-positive cells in blood were determined by flow cytometry using antibodies to CD45.1 Clone A20, CD45.2 Clone 104, Gr1 Clone RB6–8C5, CD115 Clone AFS98, and/or CD3 Clone 17A, CD4 Clone GK1.5 and CD45R Clone RA3–6B2.

scRNA-seq

For single-cell suspensions, cleaned aortas (ascending and arch) were minced and digested as previously described[12]. Aortas were briefly digested with 2.5 mg ml^{-1} Liberase (Millipore Sigma, LIBTM-RO), 160 U ml^{-1} deoxyribonuclease I (Millipore Sigma, DN25) and 120 U ml^{-1} hyaluronidase (Millipore Sigma, H3506) with 10 μM necrosulfonamide (R&D Systems, 5025) in DMEM:F12 for 45 min, rotating at 37 °C. Suspensions were then diluted with DMEM:F12 with 10% FBS, washed and resuspended in PBS with EDTA 2 mM and 2% BSA. When indicated, cells were incubated with either CD45 antibodies (*Dre-Jak2*^{VF} studies) or none and then washed. Cells were then incubated with DAPI and Vibrant DyeCycle Ruby Stain and sorted based on DAPI-negative, Vibrant DyeCycle Ruby Stain (Thermo Fisher, V10309)-positive +/−ZsGreen1 and submitted for scRNA-seq. For *Dre-Jak2*^{VF} studies, cells were sorted for DAPI-negative CD45^{+} cells. After sorting, cell suspensions were incubated with CITE-seq antibodies (Biolegend CD45.1, cat. no. 110755

and CD45.2, cat. no. 109859 for Dre progression studies and Biolegend TotalSeq-A panel 750002548 for regression studies), washed and submitted for library preparation.

scRNA-seq analysis.—FASTQ files were processed with Cell Ranger v.5.0.1 and v.6.1.2, respectively, for *Tet2* and *Jak2*^{VF} scRNA-seq data. The sequencing reads were aligned to the mm10–2020-A reference transcriptome (GENCODE vM23/Ensembl98). The Cell Ranger estimated an average of 5,082 cells with 2,321 median genes per cell. The UMI count matrix obtained for each sample was analyzed using Seurat v.4.0.3 (ref. 46) in R software v.4.1.0. To control for quality of data, genes expressed in fewer than ten cells and cells expressing fewer than 200 genes and containing greater than 10% mitochondrial reads were discarded. Additional filtering parameters were also applied for each sample based on sequencing depth and are summarized in Supplementary Table 6. For each dataset, gene counts were normalized relative to the total counts in each cell, and the outputs were then multiplied by 10,000 and natural log-transformed. Downstream analyses were performed using 2,000 highly variable genes per sample. Seurat integration was utilized to minimize batch effect and the top 2,000 highly variable genes across samples were selected for integration. In *Tet2* scRNA-seq, the first 20 principal components and 25 nearest neighbors were used for the Shared Nearest Neighbor graph and 0.45 resolution was applied to identify the heterogeneous cell types based on Louvain clustering. In *Jak2*^{VF} scRNA-seq, the Shared Nearest Neighbor graph was generated from the first 30 principal components with 40 nearest neighbors and a resolution parameter of 0.7 was used to identify cell types on Uniform Manifold Approximation and Projection (UMAP). Differential gene expression analyses were conducted using Wilcoxon Rank Sum test with Bonferroni correction, and the top differentially expressed genes were obtained by comparing a cluster with all of the other clusters. Genes expressed in more than 25% of cells with at least 1.5-fold difference and Bonferroni corrected *P* value of less than 0.05 were defined as being differentially expressed for each cell type.

CITE-seq analysis.—All feature barcode data were processed with Cell Ranger v.5.0.1. Five antibodies from TotalSeq-B and 119 antibodies from TotalSeq-A panels were used to detect surface proteins, respectively, in *Dre-Jak2*^{VF} bone marrow and regression CITE-seq data. Averages of the Cell Ranger outputs had 6,341 cells and 1,330 median genes per cell. Multimodal analysis was performed to utilize both cellular transcriptomes and cell-surface proteins from the same cell in CITE-seq data. Both CITE-seq data were first preprocessed (Supplementary Table 7) and clustered based on the measured RNA UMI matrix and cell-surface protein expression was visualized in each cluster. In *Dre-Jak2*^{VF} CITE-seq, 6,331 cells with antibody-derived tag UMI counts greater than 8 for either CD45.1 or CD45.2 were used for the subsequent analyses, to prevent cells expressing both CD45 surface proteins from engaging in the analyses. Seurat SCTransform[47] was implemented to normalize and stabilize the variance of each dataset. Then, 1,500 highly variable genes were selected to integrate the three datasets and single cells were clustered based on 20 principal components and 0.8 resolution. Five surface protein markers from antibody-derived tag data were then normalized using a centered log ratio transformation to visualize expression on clusters obtained from RNA profiles. In regression CITE-seq, 12 cells with a total UMI count of 9 isotype control antibodies >50 were discarded. A total of 13,057 cells were

normalized and the samples were then integrated based on 2,000 highly variables genes. Fifteen principal components and 0.6 resolution were set to cluster cells on the basis of cellular transcriptomes. Then, 110 surface protein markers were normalized applying a centered log ratio transformation. Differentially expressed genes and proteins expressed in more than 25% of cells in either group with at least 1.5-fold difference were identified by comparing a cluster with all of the others separately by RNA and protein levels.

Analysis of regression CITE-seq myeloid cells.—Clustering analysis of myeloid cells in the Dre-*Jak2*^{VF} regression study was also performed in Seurat. In total, 6,123 cells from macrophages, monocytes and dendritic cells identified by RNA profile were extracted and log-normalized for the subsequent clustering analysis. Then, 1,000 highly variable genes across samples were used to re-integrate the myeloid cells. Ten principal components and 30 nearest neighbors were used with 0.4 resolution to identify ten cell clusters. Expression of centered log ratio-transformed surface protein markers was then visualized in UMAP. Differentially expressed genes and proteins expressed in more than 25% of cells with greater than 1.5-fold difference were identified separately in RNA and protein profiles.

Statistics

Sample sizes are reported in figure legends. All *n* values are based on individual mice or patients, not repeated measures. All statistical tests were two-sided unless otherwise indicated. Data normality was tested in all samples by a Kolmogoov–Smirnov test using Prism 9 software. All *P* values for statistical tests examining more than two groups were adjusted for multiple comparisons. Statistical analysis was conducted with GraphPad Prism 9 and Microsoft Excel.

Extended Data

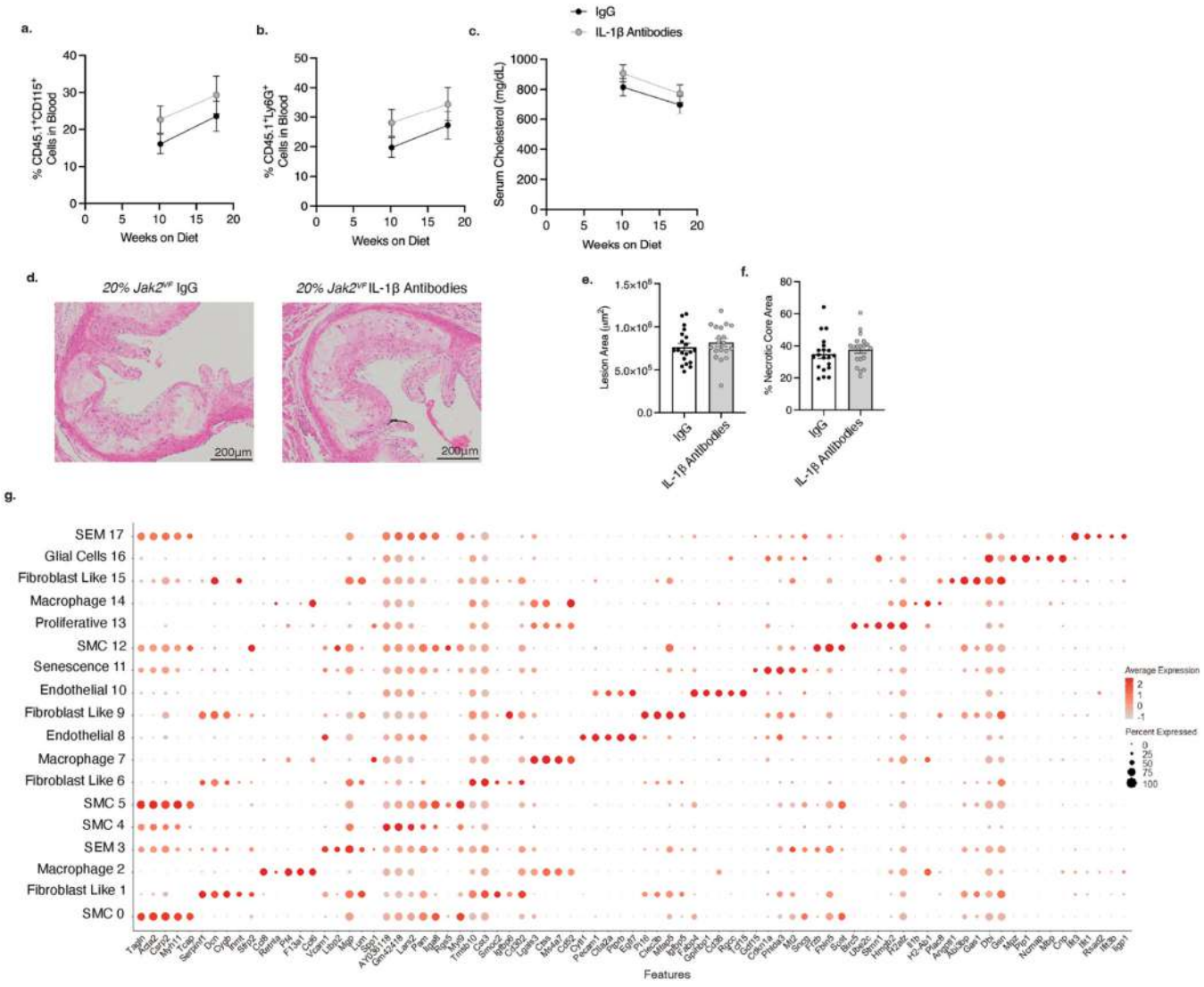

Extended Data Fig. 1 |. IL-1β inhibition does not alter smooth muscle cell differentiation. Quantification of *Jak2*^{VF} burden (CD45.1^{+} cells) in blood **a**. monocytes and **b**. neutrophils (n = 19 IgG, n = 20 IL-1β antibodies). **c**. Serum Cholesterol (n = 20 IgG, n = 19 IL-1β antibodies) **d**. Representative H&E image of aortic root lesions of mice modeling *Jak2*^{VF}-CH treated with IgG or IL-1β antibodies. Quantification of **e**. lesion area and **f**. percent necrotic core area (n = 20 IgG, n = 19 IL-1β antibodies). **g**. Differential gene expression of the top 5 genes expressed per cluster from scRNA-Seq analysis of mice modeling *Jak2*-CH (related to Fig. 2j-l). Data are mean ± SEM. Two-Way ANOVA; **a**, **b**, & **c**. Two-tailed Students t-test **e** & **f**.

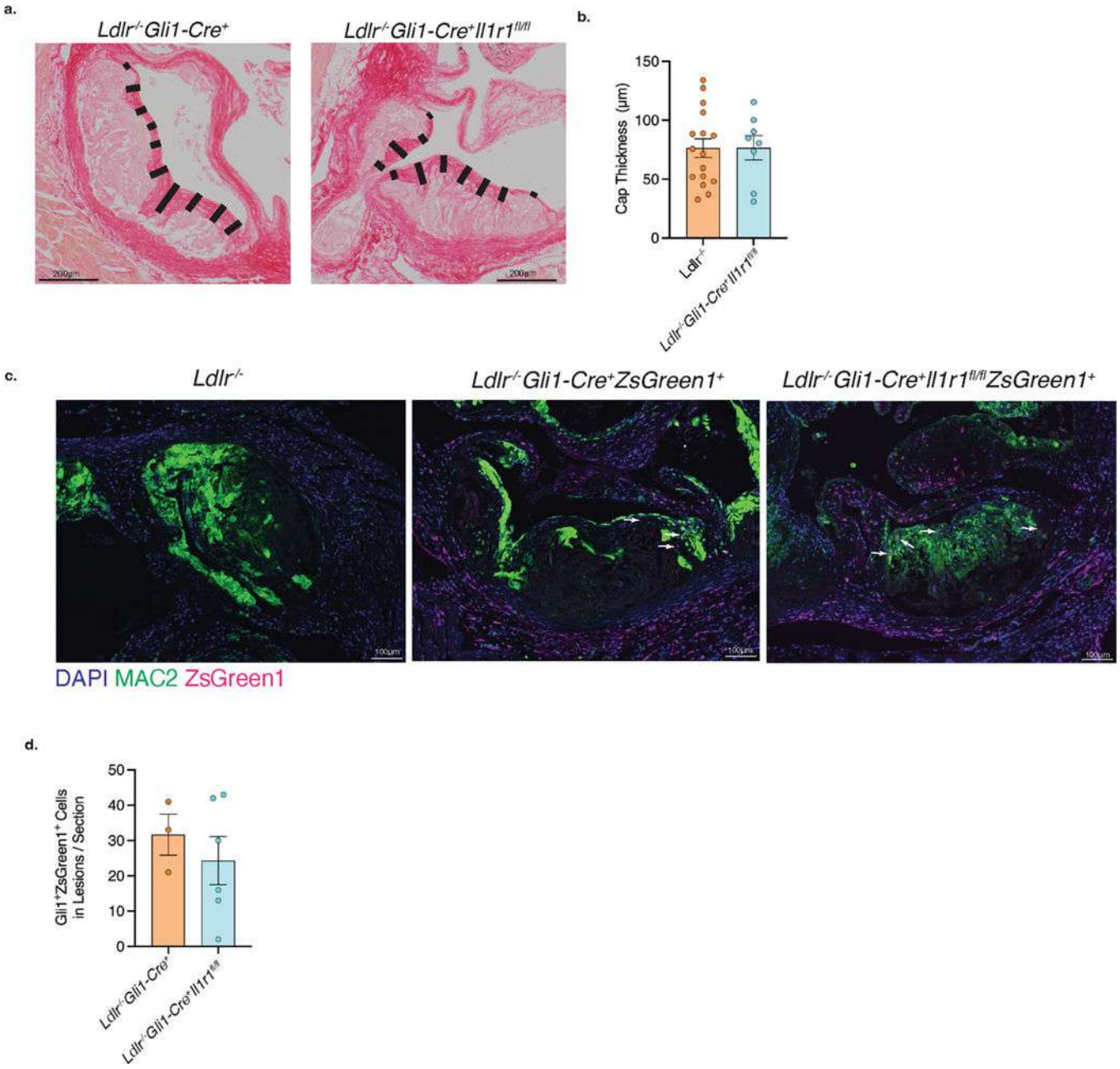

Extended Data Fig. 2 |. IL-1 signaling in mesenchymal stem cell derived cells does not regulate cap thickness.

Recipient mice with the indicated genotypes were transplanted with 20% *Jak2*^{VF} bone marrow to model clonal hematopoiesis. Mice were fed a western type of diet for 12 weeks then lesions were analyzed. **a**. Representative picrosirius red image of aortic root lesions from mice modeling *Jak2*^{VF} CH with the indicated genotypes, black bar indicates cap thickness. **b**. Quantification of cap thickness (Ldlr$^{-/-}$Gli1-Cre^{+} n = 16, Ldlr$^{-/-}$Gli1-Cre^{+}ll1r1$^{fl/fl}$ n = 8). **c**. Immunofluorescent images of lesions from mice with the indicated genotypes, white arrows indicate Gli1-ZsGreen1^{+} cells in intima; ZsGreen1 Positive cells are Magenta. **d**. Quantification of Gli1-ZsGreen1^{+} in atheromas (Ldlr$^{-/-}$Gli1-

$Cre^{+}ZsGreen1^{+}$ n = 3, $Ldlr^{-/-}Gli1\text{-}Cre^{+}ll1r1^{fl/fl}$ $ZsGreen1^{+}$ n = 6). Data are mean ± SEM. Two-tailed Students t-test **b**. Two-tailed Mann-Whitney test **d**.

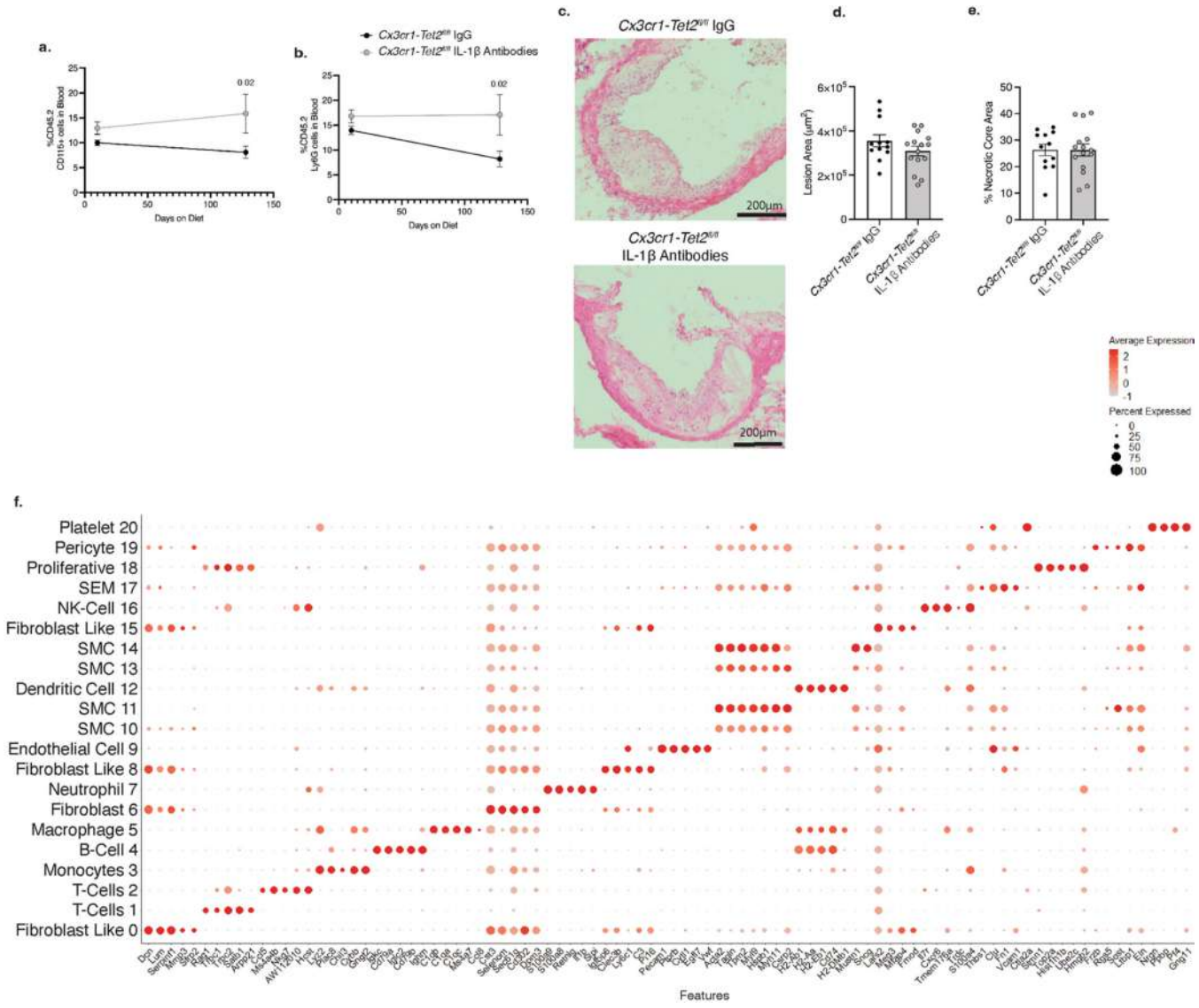

Extended Data Fig. 3 |. IL-1β inhibition in mice with monocyte/macrophage restricted deletion of *Tet2 Cx3cr1-Tet2*$^{fl/fl}$.

Percent of cells lacking *Tet2* in blood ($CD45.2^{+}$ cells) **a**. Monocytes and **b**. neutrophils (n = 12 IgG, n = 15 IL-1β antibodies). **c**. Representative H&E image of aortic root lesions from mice lacking *Tet2* in monocytes and macrophages treated with IgG or IL-1β antibodies as outlined in Fig. 2a. Quantification of **d**. lesion area and **e**. Percent necrotic core area (n = 12 IgG, n = 15 IL-1β antibodies). **f**. Differential gene expression of the top 5 genes expressed per cluster from scRNA-seq analysis of mice with *Tet2* deletion (related to Fig. 4e-g). Data are mean ± SEM. Two-Way ANOVA **a** & **b**. Two-tailed Students t-test **d** & **e**.

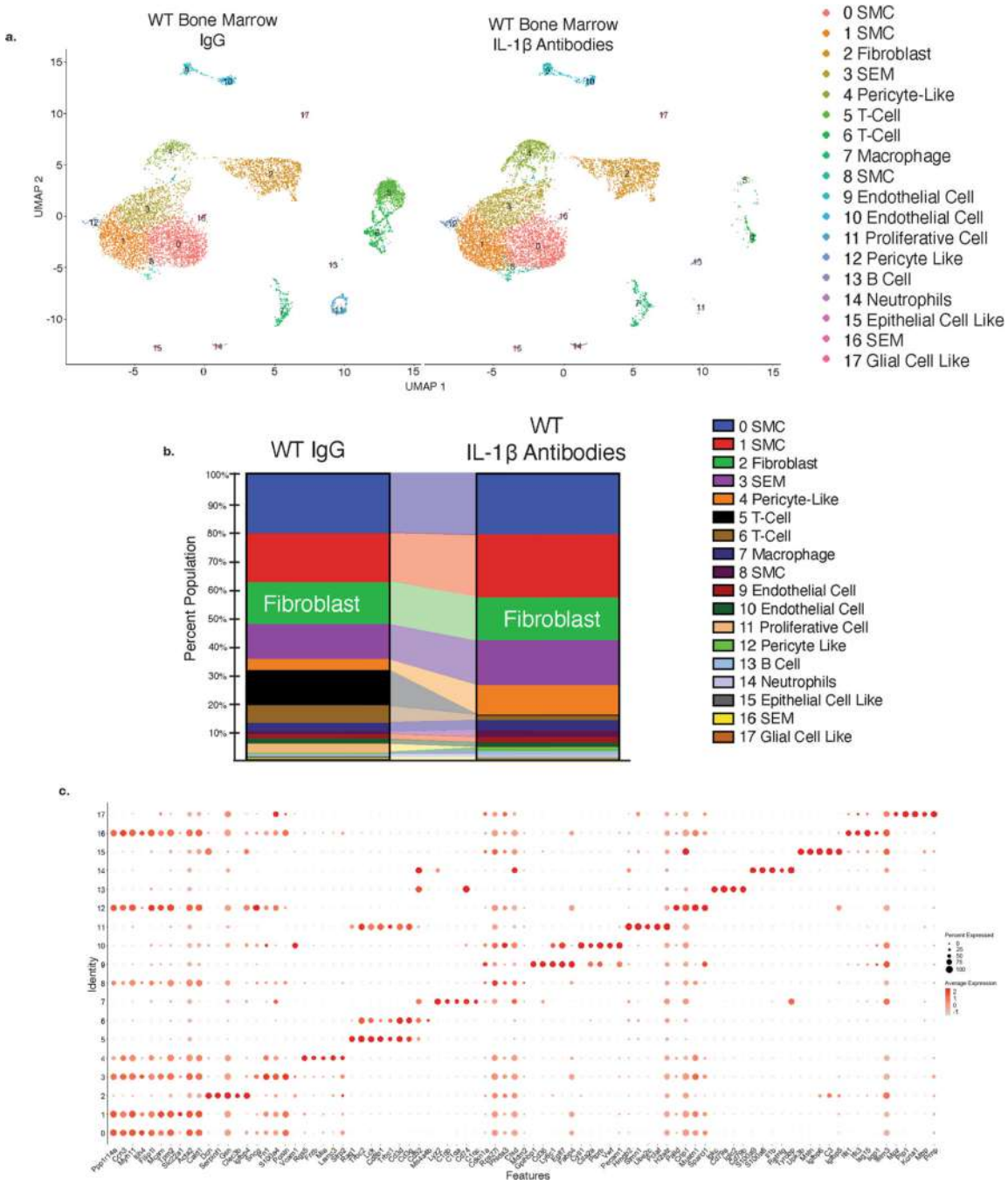

Extended Data Fig. 4 |. Fibroblast-like cells do not expand in lesions of mice with WT bone marrow.

Ldlr$^{-/-}$ mice were transplanted with WT bone marrow and subjected to a 10-week western type diet, then administered IgG or Il-1β antibodies for an addition 7 weeks with western type diet feeding. Aortas were then isolated for scRNA-Sequencing. **a**. UMAP visualization of cells isolated from aortas; Stem cell, endothelial cell, monocyte like cell (SEM). **b**. scRNA-Seq population distribution across. **c**. Differential gene expression of the top 5 genes expressed per cluster from scRNA-seq analysis of mice with WT bone marrow.

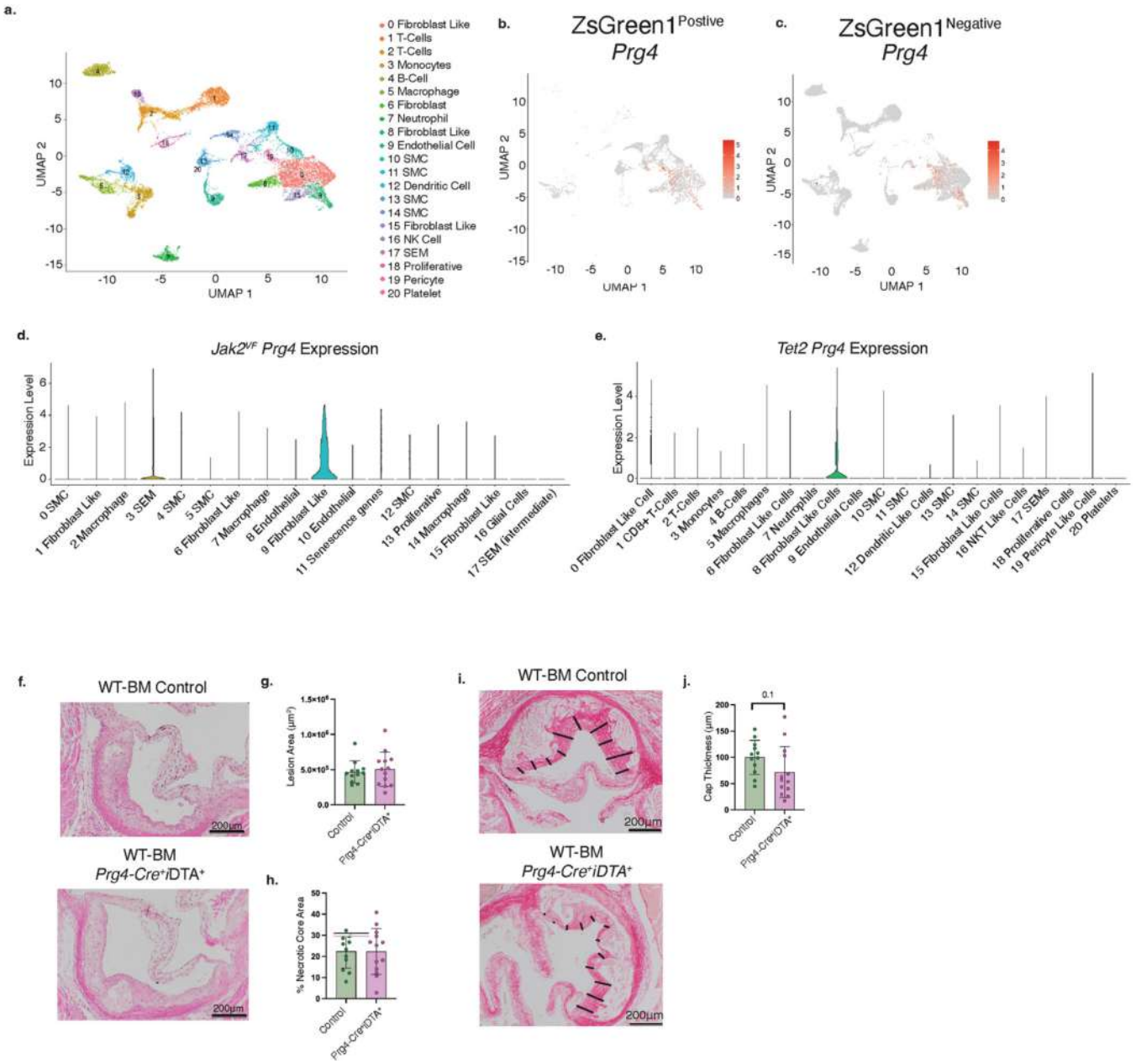

Extended Data Fig. 5 |. *Prg4* is primarily expressed in fibroblast-like cells.

a. UMAP visualization of scRNA-Seq from aortas modeling *Tet2*-CH overlay with *Prg4* expression in **b**. Zsgreen1^{+} and **c**. ZsGreen1^{Neg} populations. **d**. Violin plot of *Prg4* expression in all clusters from mice modeling **d**. *Jak2*^{VF}-CH and **e**. *Tet2*-CH. **f**. Representative H&E image of aortic roots of mice with WT bone marrow (BM) and the indicated genotype. Quantification of **g**. Lesion area and **h**. Percent necrotic core area (n = 12 *Ldlr*$^{-/-}$ *Prg4-Cre*$^{+}$, n = 13 *Ldlr*$^{-/-}$ *Prg4-Cre*$^{+}$ *iDTA*$^{+}$). **i**. Representative picrosirius red staining of aortic root lesions, black bar indicates cap thickness. **j**. Quantification of cap thickness (n = 12 Ldlr$^{-/-}$ *Prg4-Cre*$^{+}$, n = 13 *Ldlr*$^{-/-}$ *Prg4-Cre*$^{+}$ *iDTA*$^{+}$). Data are mean ± SEM. Two-tailed Students t-test **g**, **h**, & **j**.

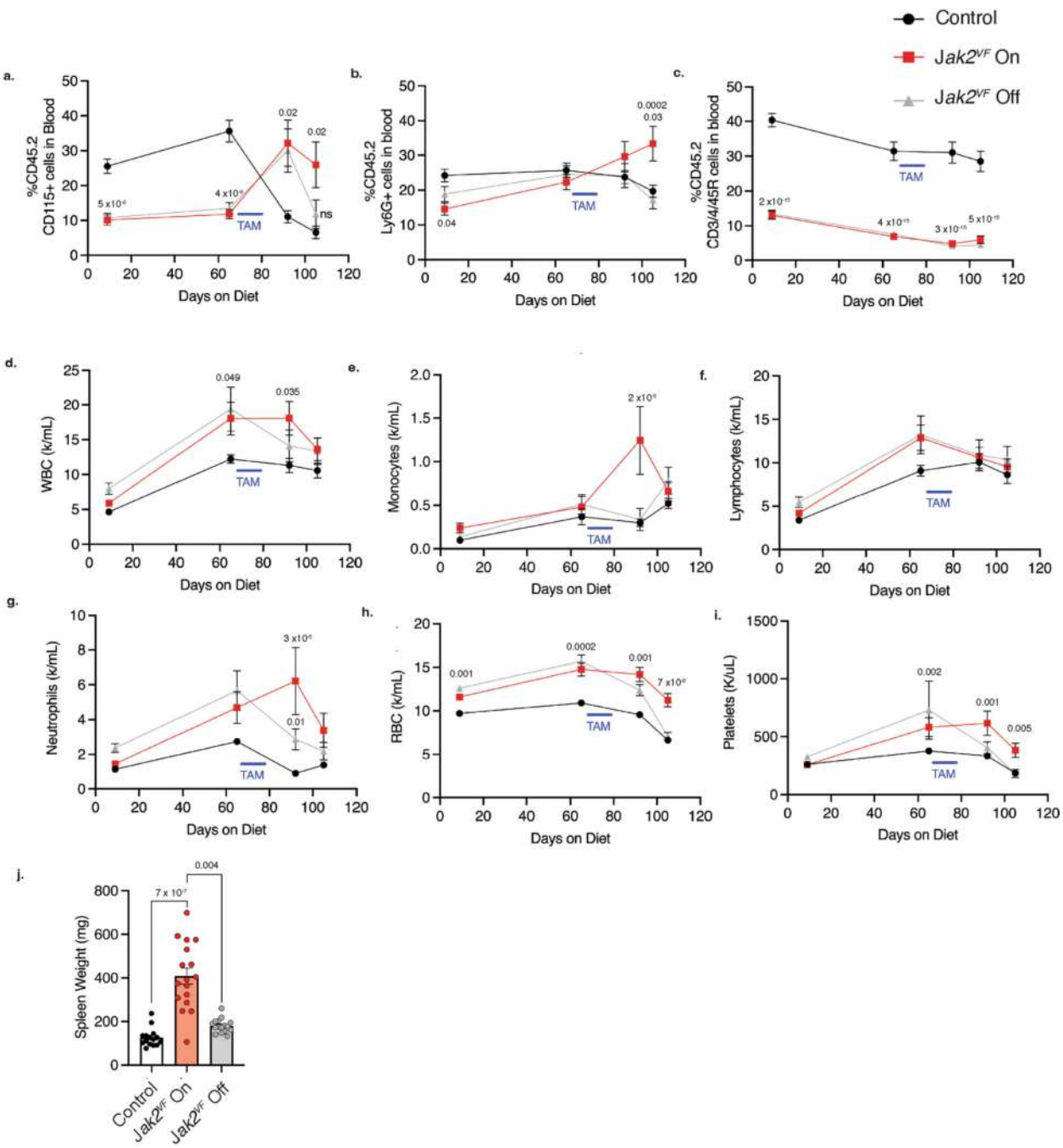

Extended Data Fig. 6 |. Hematopoietic cells in *Dre-Jak2*^{VF} mice.

Percent *Jak2*^{VF} (CD45.2^{+}) **a**. monocytes, **b**. Neutrophils, **c**. Lymphocytes in blood (n = 15 Control, n = 17 *Jak2*^{VF} On, n = 16 J*ak2*^{VF} Off), TAM indicates administration of tamoxifen diet to control and *Jak2*^{VF} Off mice. Blood cells counts of **d**. White blood cells (WBC), **e**. monocytes, **f**. Lymphocytes, **g**. Neutrophils, **h**. RBCs, and **i**. Platelets (n = 15 Control, n = 17 *Jak2*^{VF} On, n = 16 *Jak2*^{VF} Off). **j**. Spleen weight of mice related to Fig. 4b-d (n = 15 Control, n = 17 *Jak2*^{VF} On, n = 16 *Jak2*^{VF} Off). Data are mean ± SEM. Two-Way ANOVA with Tukey post hoc analysis **a-i**. Kruskal-Wallis test with Dunn's multiple comparisons **j**.

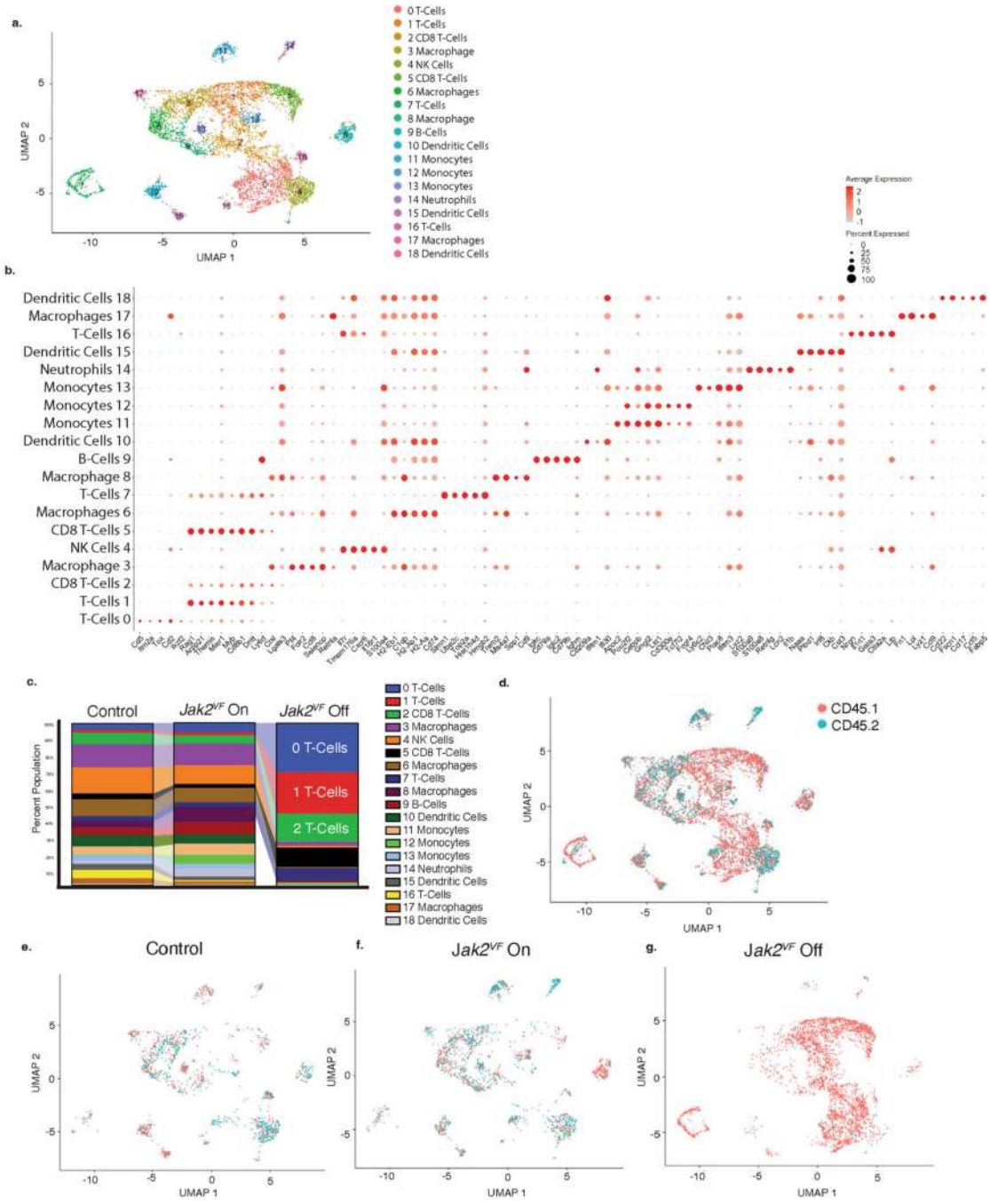

Extended Data Fig. 7 |. scRNA-seq analysis of *Dre-Jak2*^{VF} plaques.

a. UMAP visualization of scRNA-seq analysis of CD45.1/2^{+} cells from aortas of mice modeling CH with *Dre-Jak2*^{VF}. **b**. Differential gene expression of the top 5 genes expressed/cluster from scRNA-Seq analysis. **c**. Proportion of cells identified with scRNA-seq. **d**. UMAP visualization of scRNA-seq overlay with CD45.1 & CD45.2 barcoded antibodies to indicate *Dre-Jak2*^{VF} status within **e**. Control, **f**. *Jak2*^{VF} On and **g**. *Jak2*^{VF} Off lesions, each sample are 5 pooled mice.

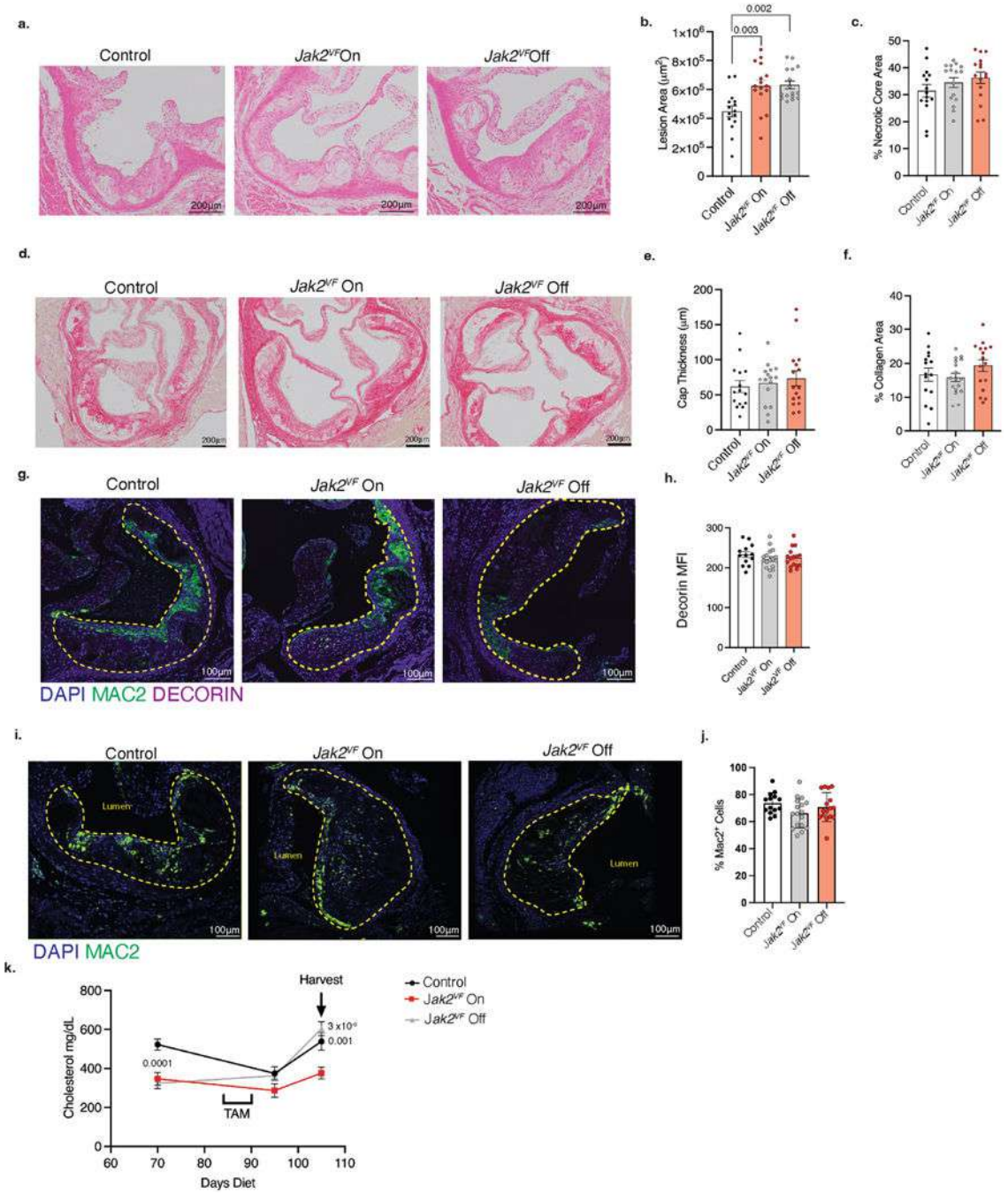

Extended Data Fig. 8 |. Features of plaque stability are unchanged in Dre-*Jak2*^{VF} lesions.

a. Representative H&E images of aortic root lesions from mice with continuous *Jak2*^{VF} expression (*Jak2*^{VF} On) and mice that turn *Jak2*^{VF} Off with tamoxifen (TAM) administration (*Jak2*^{VF} Off), TAM chow was administered to control and *Jak2*^{VF} Off groups. Quantification of **b**. lesion area and **c**. percent necrotic core area (n = 15 Control, n = 16 *Jak2*^{VF} On, n = 16 *Jak2*^{VF} Off). **d**. Representative picrosirius red stained aortic root lesions. Quantification of **e**. Cap thickness and **f**. collagen area marked by picrosirius red staining (n = 15 Control, n = 17 *Jak2*^{VF} On, n = 16 *Jak2*^{VF} Off). **g**. Immunofluorescence (IF) staining of aortic root lesions.

h. Quantification of Decorin mean fluorescence intensity (MFI) in lesions (n = 13 Control, n = 17 *Jak2*^{VF} On, n = 16 *Jak2*^{VF} Off). **i**. IF staining of aortic root lesions. **j**. Quantification of macrophage density marked by percent MAC2^{+} cells in lesions (n = 14 Control, n = 17 *Jak2*^{VF} On, n = 17 *Jak2*^{VF} Off) **k**. Serum cholesterol levels (n = 15 Control, n = 17 *Jak2*^{VF} On, n = 16 *Jak2*^{VF} Off). mice. Data are mean ± SEM. One-Way ANOVA with Tukey's post-hoc analysis **b**, **c**, **e**, **f**, **h**, & **j**). Two-Way ANOVA with Tukey's multiple comparison test **k**.

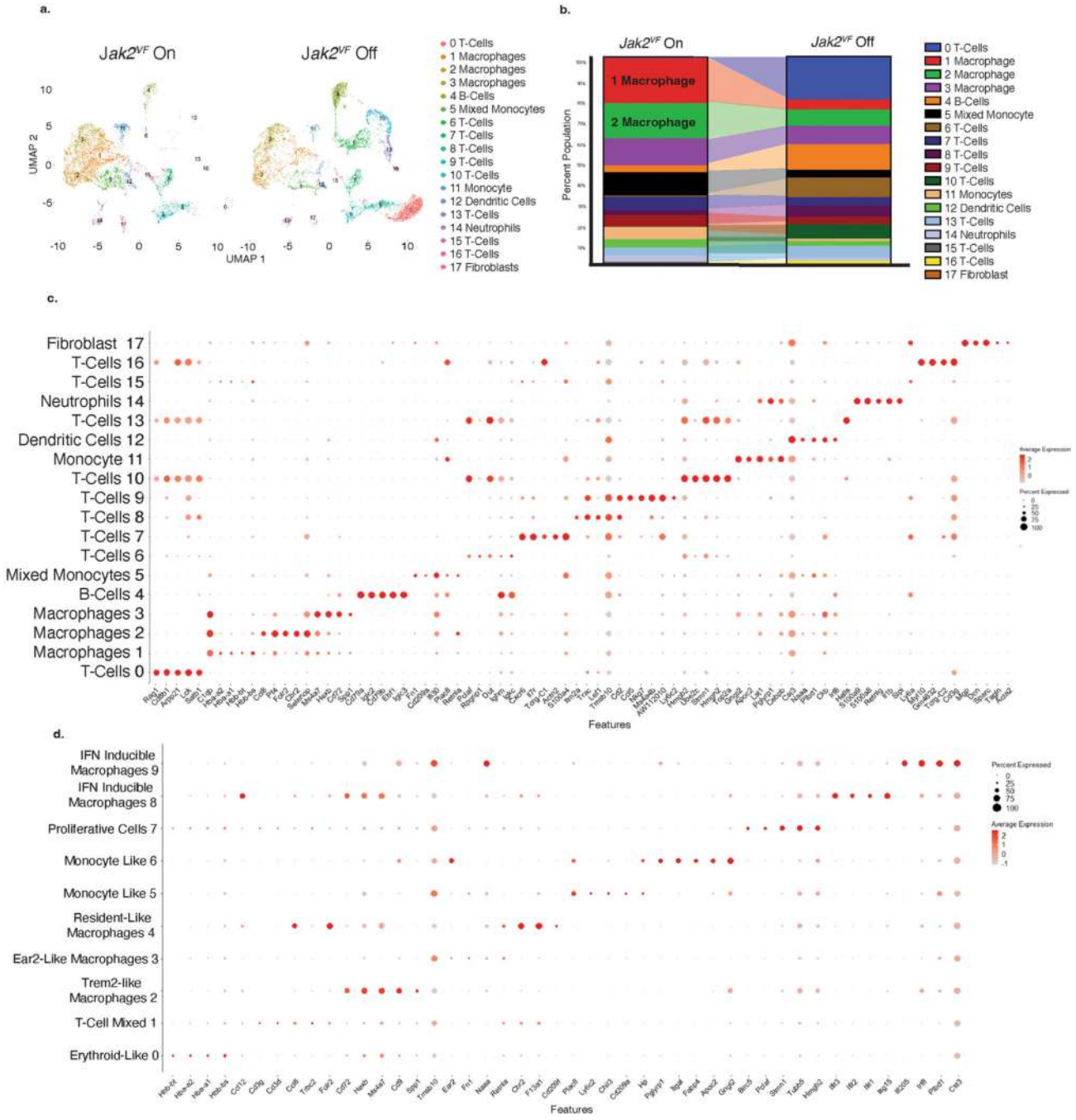

Extended Data Fig. 9 |. Turning *Jak2*^{VF} Off in conjunction with cholesterol lowering alters immune cell composition.

a. UMAP visualization of scRNA-Seq of aortic cells following cholesterol lowering. **b**. Population distribution of scRNA-Seq analysis. **c**. Differential gene expression of the top 5 genes expressed per cluster from scRNA-Seq analysis. **d**. Differential gene expression of the top 5 genes expressed per cluster from scRNA-Seq analysis of CD45^{+} myeloid cells.

Supplementary Material

Refer to Web version on PubMed Central for supplementary material.

Acknowledgements

This work was supported by the Leducq Foundation (TNE-18CVD04) and National Institutes of Health (NIH) grants no. HL155431, no. HL170157 and no. HL107653 (to A.R.T.). T.P.F. was supported by grants no. F32HL151051-01 and no. K99HL157649, and grant no. R00HL157649 from the NIH, as well as a Mandl Connective Tissue Research Fellowship. R.L. was supported by National Cancer Institute grant no. R35 CA197594 and NIH/NCI Cancer Center Support Grant no. P30 CA008748. A.D. is a William Raveis Charitable Fund Physician-Scientist of the Damon Runyon Cancer Research Foundation (grant no. PST-24-19). He also has received funding from the American Association of Cancer Research (grant no. 17-40-11-DUNB) and the American Association of Clinical Oncology (grant no. 11520). We thank the staff of the Columbia Stem Cell Initiative Flow Cytometry Core Facility, under the leadership of M. Kissner, at Columbia University Irving Medical Center for their contributions to the work presented in this manuscript. Research reported in this publication was performed in the CCTI Flow Cytometry Core, supported in part by the Office of the Director, NIH, under awards no. S10RR027050 and no. S10OD020056. The content is solely the responsibility of the authors and does not necessarily represent the official views of the NIH. Images were collected and/or image processing and analysis for this work was performed in the Confocal and Specialized Microscopy Shared Resource of the Herbert Irving Comprehensive Cancer Center at Columbia University, supported by NIH grant no. P30 CA013696.

R.L. is on the supervisory board of Qiagen and is a scientific advisor to Imago, Mission Bio, Zentalis, Ajax, Auron, Prelude, C4 Therapeutics and Isoplexis. He receives research support from Ajax and Zentalis and has consulted for Incyte, Janssen, Astra Zeneca and Novartis. He has received honoraria from Astra Zeneca, Roche, Lilly and Amgen for invited lectures and from Gilead for grant reviews. A.R.T. is on the SABs of Tensixteen Bio, and Beren Pharmaceuticals. A.D. has served on an advisory committee for Incyte. L.M. is a scientific consultant and medical advisor for Roche Diagnostics, Novo Nordisk and DrugFarm Inc., and is an advisory board member of Angiolutions. He further received research funding from Roche Diagnostics and Novo Nordisk.

Data availability

The datasets generated and/or analyzed during the current study are available in the Gene Expression Omnibus with SuperSeries no. GSE248395 and the following accession numbers: scRNA-seq of Myh11Zsgreen1 mice modeling *Jak2*^{VF} CH (Fig. 2), *Tet2* CH (Fig. 4) and mice with WT bone marrow (Extended Data Fig. 4) (GSE248394); scRNA-seq of Dre-*Jak2*^{VF} in atherosclerosis progression (Extended Data Fig. 8) (GSE248289) and Dre-*Jak2*^{VF} in atherosclerosis regression (Fig. 8) (GSE248276); scRNA-seq data of human atheromas (Fig. 1) (GSE247238). Source data are provided with this manuscript.

References

1. Tsao CW et al. Heart disease and stroke statistics—2022 update: a report from the American Heart Association. Circulation 145, e153–e639 (2022). [PubMed: 35078371]
2. Virmani R, Burke AP, Farb A. & Kolodgie FD Pathology of the vulnerable plaque. J. Am. Coll. Cardiol 47, C13–C18 (2006). [PubMed: 16631505]
3. Wirka RC et al. Atheroprotective roles of smooth muscle cell phenotypic modulation and the TCF21 disease gene as revealed by single-cell analysis. Nat. Med 25, 1280–1289 (2019). [PubMed: 31359001]

4. Grootaert MOJ, Finigan A, Figg NL, Uryga AK & Bennett MR SIRT6 protects smooth muscle cells from senescence and reduces atherosclerosis. Circ. Res 128, 474–491 (2021). [PubMed: 33353368]
5. Ridker PM et al. Antiinflammatory therapy with canakinumab for atherosclerotic disease. N. Engl. J. Med 377, 1119–1131 (2017). [PubMed: 28845751]
6. Svensson EC et al. TET2-driven clonal hematopoiesis and response to canakinumab: an exploratory analysis of the CANTOS randomized clinical trial. JAMA Cardiol. 7, 521–528 (2022). [PubMed: 35385050]
7. Tardif JC et al. Efficacy and safety of low-dose colchicine after myocardial infarction. N. Engl. J. Med 381, 2497–2505 (2019). [PubMed: 31733140]
8. Nidorf SM et al. Colchicine in patients with chronic coronary disease. N. Engl. J. Med 383, 1838–1847 (2020). [PubMed: 32865380]
9. Jones AV et al. Widespread occurrence of the JAK2 V617F mutation in chronic myeloproliferative disorders. Blood 106, 2162–2168 (2005). [PubMed: 15920007]
10. Bick AG et al. Inherited causes of clonal haematopoiesis in 97,691 whole genomes. Nature 586, 763–768 (2020). [PubMed: 33057201]
11. Jaiswal S. et al. Clonal hematopoiesis and risk of atherosclerotic cardiovascular disease. N. Engl. J. Med 377, 111–121 (2017). [PubMed: 28636844]
12. Fidler TP et al. The AIM2 inflammasome exacerbates atherosclerosis in clonal haematopoiesis. Nature 592, 296–301 (2021). [PubMed: 33731931]
13. Westerterp M. et al. Cholesterol efflux pathways suppress inflammasome activation, NETosis, and atherogenesis. Circulation 138, 898–912 (2018). [PubMed: 29588315]
14. Yu Z. et al. Genetic modification of inflammation and clonal hematopoiesis-associated cardiovascular risk. J. Clin. Invest 10.1172/JCI168597 (2023).
15. Aragam KG et al. Discovery and systematic characterization of risk variants and genes for coronary artery disease in over a million participants. Nat. Genet 54, 1803–1815 (2022). [PubMed: 36474045]
16. Bennett MR, Sinha S. & Owens GK Vascular smooth muscle cells in atherosclerosis. Circ. Res 118, 692–702 (2016). [PubMed: 26892967]
17. Pan H. et al. Single-cell genomics reveals a novel cell state during smooth muscle cell phenotypic switching and potential therapeutic targets for atherosclerosis in mouse and human. Circulation 142, 2060–2075 (2020). [PubMed: 32962412]
18. Choudhury RP et al. Arterial effects of canakinumab in patients with atherosclerosis and type 2 diabetes or glucose intolerance. J. Am. Coll. Cardiol 68, 1769–1780 (2016). [PubMed: 27737744]
19. Gomez D. et al. Interleukin-1β has atheroprotective effects in advanced atherosclerotic lesions of mice. Nat. Med 24, 1418–1429 (2018). [PubMed: 30038218]
20. Alexanian M. et al. Chromatin remodeling drives immune-fibroblast crosstalk in heart failure pathogenesis. Preprint at bioRxiv 10.1101/2023.01.06.522937 (2023).
21. Amrute JM et al. Targeting the immune-fibrosis axis in myocardial infarction and heart failure. Preprint at bioRxiv 10.1101/2022.10.17.512579 (2022).
22. Buechler MB et al. Cross-tissue organization of the fibroblast lineage. Nature 593, 575–579 (2021). [PubMed: 33981032]
23. Kramann R. et al. Adventitial MSC-like cells are progenitors of vascular smooth muscle cells and drive vascular calcification in chronic kidney disease. Cell Stem Cell 19, 628–642 (2016). [PubMed: 27618218]
24. Zhang X. et al. Thymosin beta 10 is a key regulator of tumorigenesis and metastasis and a novel serum marker in breast cancer. Breast Cancer Res. 19, 15 (2017). [PubMed: 28179017]
25. Kozhemyakina E. et al. Identification of a Prg4-expressing articular cartilage progenitor cell population in mice. Arthritis Rheumatol. 67, 1261–1273 (2015). [PubMed: 25603997]
26. Ytterberg SR et al. Cardiovascular and cancer risk with tofacitinib in rheumatoid arthritis. N. Engl. J. Med 386, 316–326 (2022). [PubMed: 35081280]
27. Dunbar A. et al. Jak2V617F reversible activation shows an essential requirement for Jak2V617F in myeloproliferative neoplasms. Preprint at bioRxiv 10.1101/2022.05.18.492332 (2022).

28. Liu DJ et al. Exome-wide association study of plasma lipids in >300,000 individuals. Nat. Genet 49, 1758–1766 (2017). [PubMed: 29083408]
29. Schlegel M. et al. Silencing myeloid netrin-1 induces inflammation resolution and plaque regression. Circ. Res 129, 530–546 (2021). [PubMed: 34289717]
30. Zernecke A. et al. Meta-analysis of leukocyte diversity in atherosclerotic mouse aortas. Circ. Res 127, 402–426 (2020). [PubMed: 32673538]
31. Ramachandran P. et al. Resolving the fibrotic niche of human liver cirrhosis at single-cell level. Nature 575, 512–518 (2019). [PubMed: 31597160]
32. Raber L. et al. Effect of alirocumab added to high-intensity statin therapy on coronary atherosclerosis in patients with acute myocardial infarction: the PACMAN-AMI randomized clinical trial. JAMA 327, 1771–1781 (2022). [PubMed: 35368058]
33. Nicholls SJ et al. Effect of evolocumab on coronary plaque phenotype and burden in statin-treated patients following myocardial infarction. JACC Cardiovasc. Imaging 15, 1308–1321 (2022). [PubMed: 35431172]
34. Redgrave JN, Gallagher P, Lovett JK & Rothwell PM Critical cap thickness and rupture in symptomatic carotid plaques: the Oxford plaque study. Stroke 39, 1722–1729 (2008). [PubMed: 18403733]
35. Tallquist MD Cardiac fibroblast diversity. Annu. Rev. Physiol 82, 63–78 (2020). [PubMed: 32040933]
36. Komatsu N. & Takayanagi H. Mechanisms of joint destruction in rheumatoid arthritis—immune cell-fibroblast-bone interactions. Nat. Rev. Rheumatol 18, 415–429 (2022). [PubMed: 35705856]
37. Aghajanian H. et al. Targeting cardiac fibrosis with engineered T cells. Nature 573, 430–433 (2019). [PubMed: 31511695]
38. Abplanalp WT et al. Cell-intrinsic effects of clonal hematopoiesis in heart failure. Nat. Cardiovasc. Res 10.1038/s44161-023-00322-x (2023).
39. Pelisek J. et al. Biobanking: objectives, requirements, and future challenges—experiences from the Munich Vascular Biobank. J. Clin. Med 10.3390/jcm8020251 (2019).
40. Fasolo F. et al. Long noncoding RNA MIAT controls advanced atherosclerotic lesion formation and plaque destabilization. Circulation 144, 1567–1583 (2021). [PubMed: 34647815]
41. Winter H. et al. Targeting long non-coding RNA NUDT6 enhances smooth muscle cell survival and limits vascular disease progression. Mol. Ther 31, 1775–1790 (2023). [PubMed: 37147804]
42. Mullally A. et al. Physiological Jak2V617F expression causes a lethal myeloproliferative neoplasm with differential effects on hematopoietic stem and progenitor cells. Cancer Cell 17, 584–596 (2010). [PubMed: 20541703]
43. Yurdagul A Jr. et al. Macrophage metabolism of apoptotic cell-derived arginine promotes continual efferocytosis and resolution of injury. Cell Metab. 31, 518–533.e10 (2020). [PubMed: 32004476]
44. Vromman A. et al. Stage-dependent differential effects of interleukin-1 isoforms on experimental atherosclerosis. Eur. Heart J 40, 2482–2491 (2019). [PubMed: 30698710]
45. Schindelin J. et al. Fiji: an open-source platform for biological-image analysis. Nat. Methods 9, 676–682 (2012). [PubMed: 22743772]
46. Stuart T. et al. Comprehensive integration of single-cell data. Cell 177, 1888–1902.e21 (2019). [PubMed: 31178118]
47. Hafemeister C. & Satija R. Normalization and variance stabilization of single-cell RNA-seq data using regularized negative binomial regression. Genome Biol. 20, 296 (2019). [PubMed: 31870423]

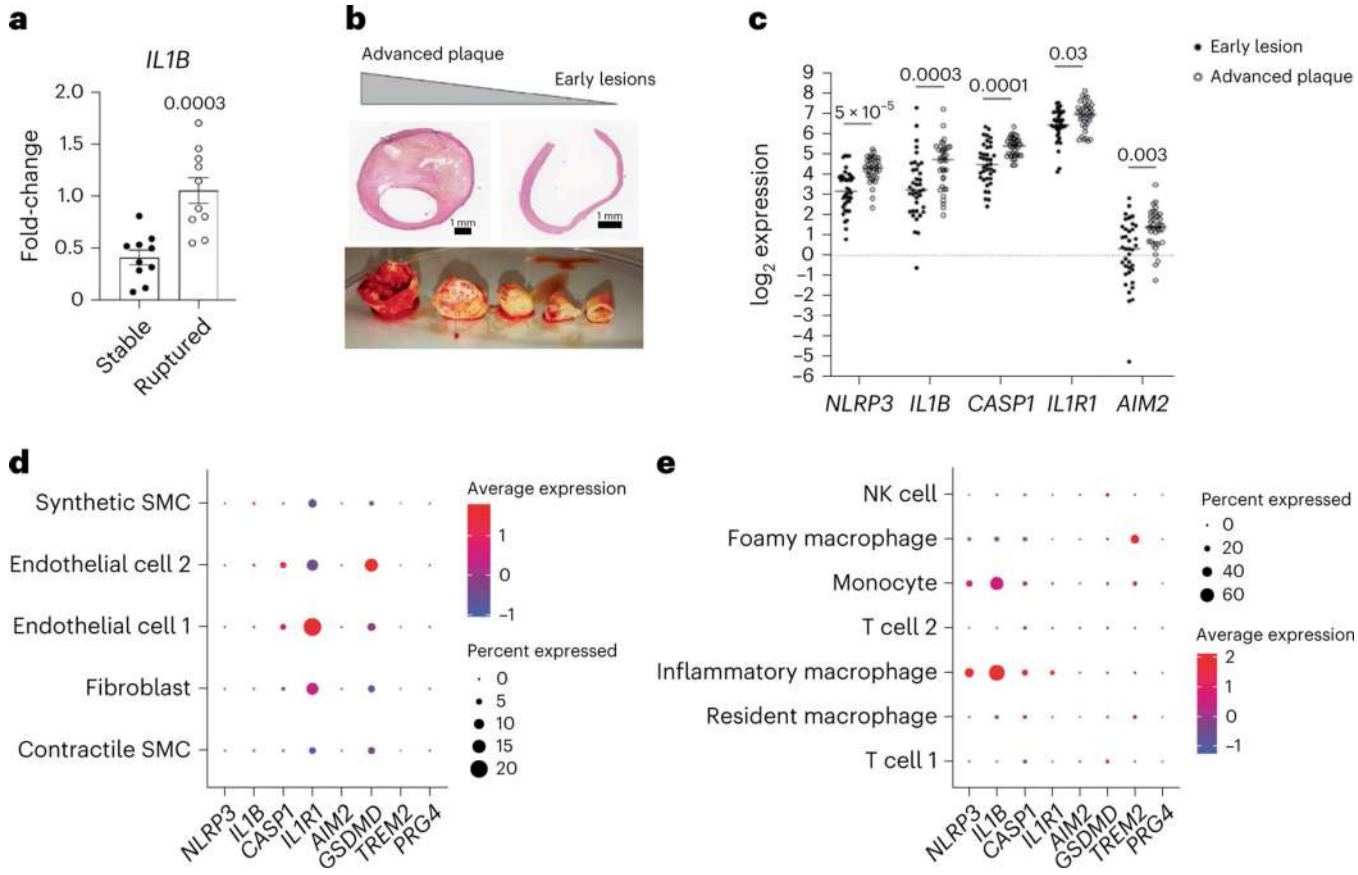

Fig. 1 |. Inflammasome components in human atheromas.

a, Quantitative PCR analysis of *IL1B* expression in cap of atheromas; data obtained from laser catapult of tissue (6 female, 14 male) ($n = 10$). **b**, Representative image of early lesions and advanced carotid plaque from the same individual (10 female, 28 male) ($n = 38$). **c**, Bulk-cell RNA expression of inflammasome-related transcripts in early and advanced human carotid lesions (10 female, 28 male) ($n = 38$). **d**,**e**, scRNA-seq of human atheromas in immune cells (**d**) and stromal cells (**e**) including SMCs; data are pooled from 10 independent experiments (1 female, 9 male) ($n = 10$). Data are mean ± s.e.m. Two-sided Mann–Whitney (**a**). Linear modeling adjusted for multiple testing (**c**). NK, natural killer.

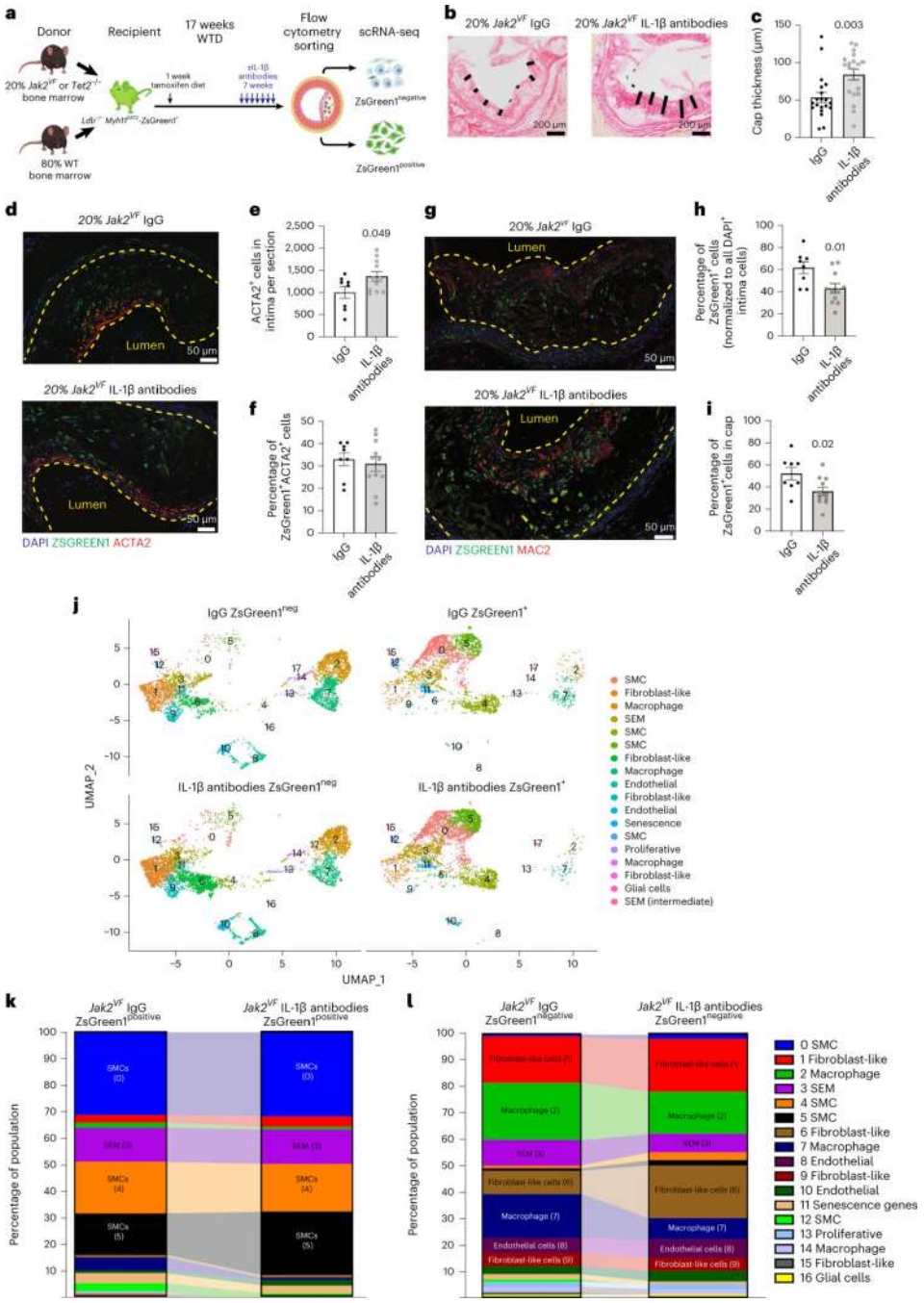

Fig. 2 |. IL-1β inhibition does not alter SMC differentiation.

a, Experimental scheme for SMC lineage tracing studies. **b**, Representative images of picrosirius red staining of lesion; black bar indicates cap thickness (n = 19). **c**, Quantification of cap thickness, n = 19. **d**, Immunofluorescence (IF) images of aortic roots; dashed yellow lines indicate lesions (n = 8 IgG, n = 11 IL-1β antibodies). **e**,**f**, Quantification of total ACTA2$^+$ cells (**e**) and the percentage of ZsGreen1$^+$ACTA2$^+$ cells (**f**) in lesions (n = 8 IgG, n = 11 IL-1β antibodies). **g**, IF images of aortic roots; dashed yellow lines indicate lesions (n = 8 IgG, n = 11 IL-1β antibodies). **h**,**i**, Quantification of percentage of total

ZsGreen1^{+} cells in lesions (**h**) and percentage of ZsGreen1^{+} cells in the cap region (**i**) (n = 8 IgG, n = 11 IL-1β antibodies). **j**, UMAP visualization of cells isolated from aortas and sorted based on ZsGreen1 status (each sample is 5 pooled mice). **k**,**l**, scRNA-seq population distribution in ZsGreen1^{+} Myh11-derived cells (**k**) and ZsGreen1^{Neg} cells (**l**). Data are mean ± s.e.m. Two-tailed Student's t-test (**c**, **e**, **f**, **h** and **i**).

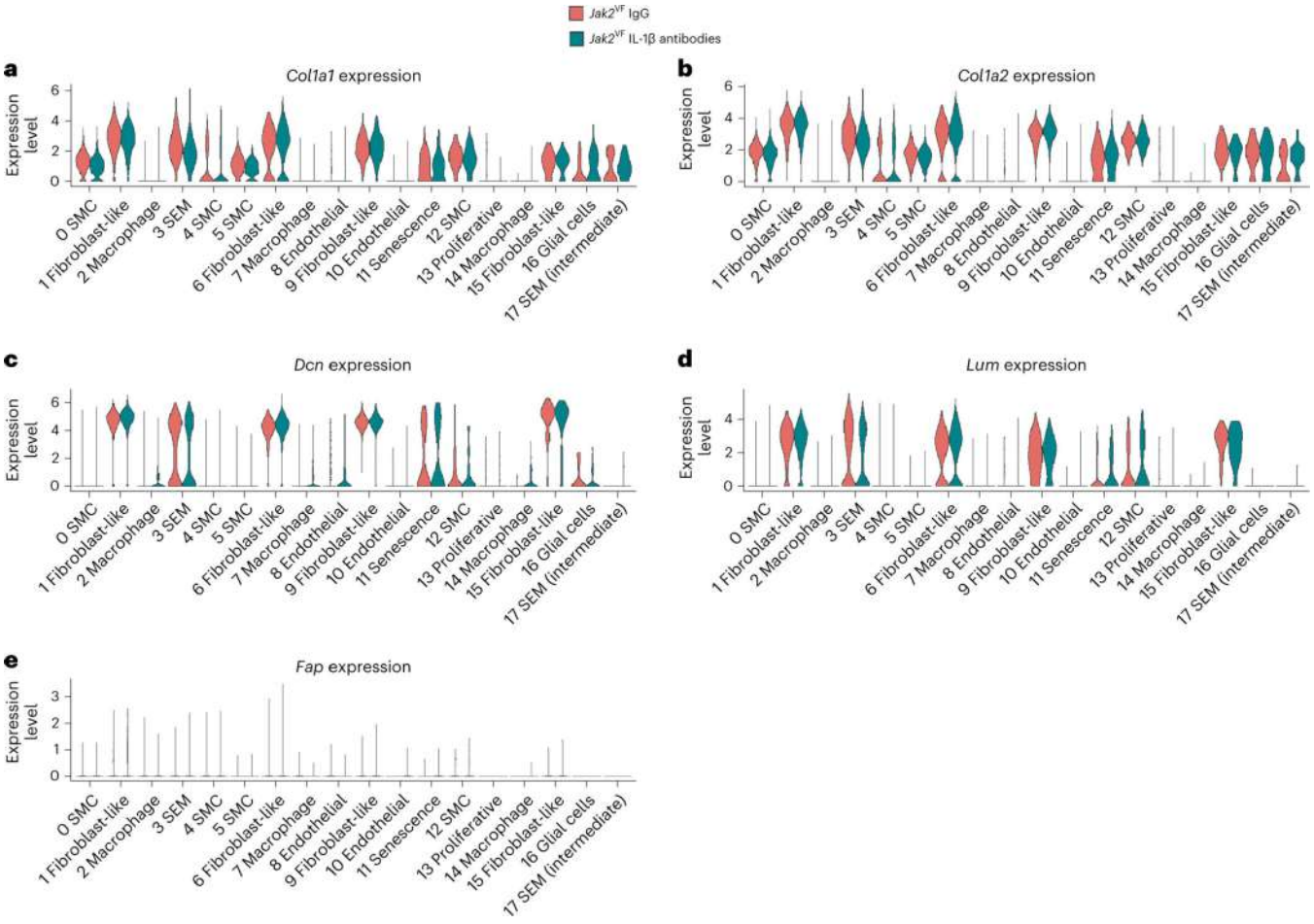

Fig. 3 |. Cluster 6 fibroblast-like cells are enriched for matrix genes in mice modeling *Jak2*^{VF} CH.
a–**e**, Violin plots of scRNA-seq data from mice modeling *Jak2*^{VF} CH for *Col1a1* (**a**), *Col1a2* (**b**), *Dcn* (**c**), *Lum* (**d**) and *Fap* (**e**).

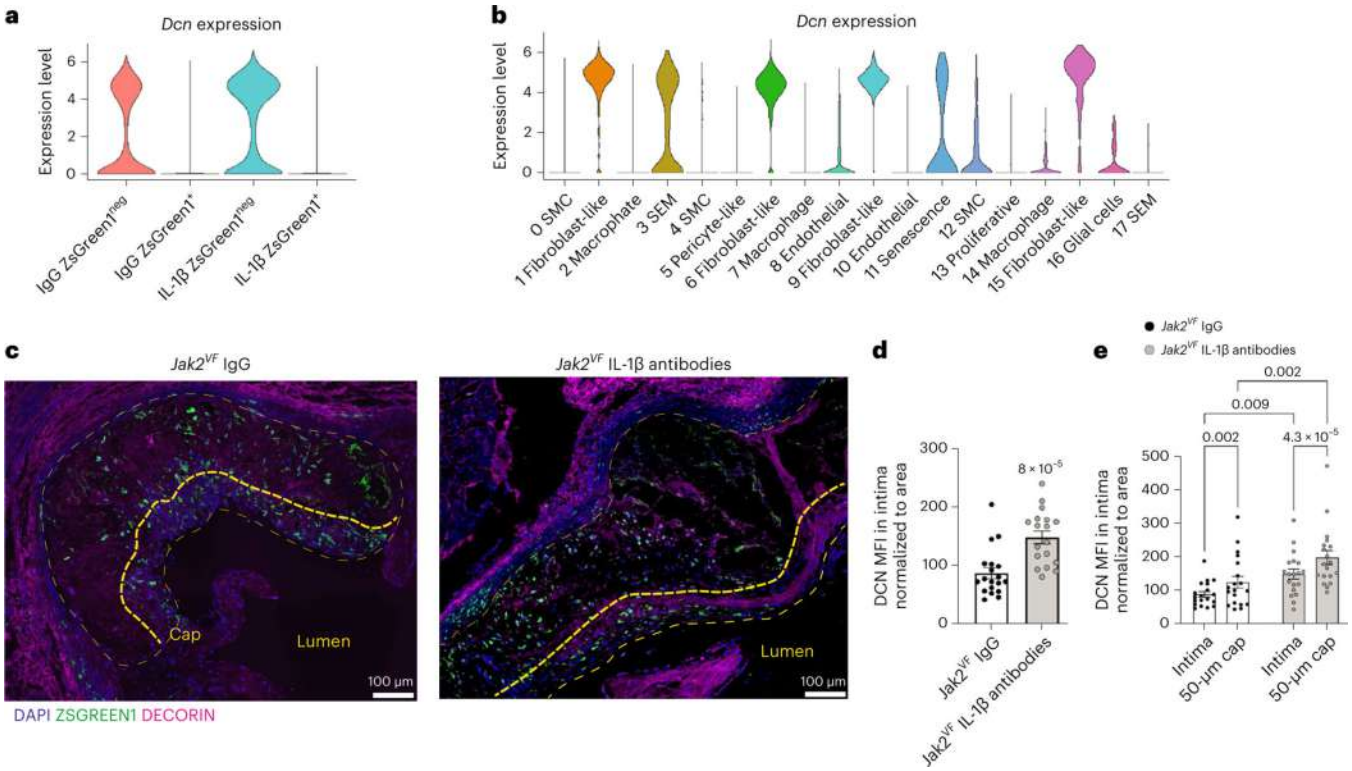

Fig. 4 |. IL-1β inhibition increases fibroblast-like cell accumulation in plaques.
a, Violin plot of *Dcn* expression based on treatment and ZsGreen1 status. **b**, *Dcn* expression in each cluster independent of ZsGreen1 and antibody status. **c**, IF images of aortic root plaques; yellow dashed lines indicate lesion, thick yellow lines indicate cap ($n = 18$). **d**,**e**, Quantification of Decorin (DCN) fluorescence in intima (**d**) ($n = 18$) and segregated by cap regions (**e**) ($n = 18$). Data are mean ± s.e.m. Mann–Whitney (**d**). Two-way analysis of variance (ANOVA) with a Sidak test (**e**). MFI, Mean Fluorescence Intensity.

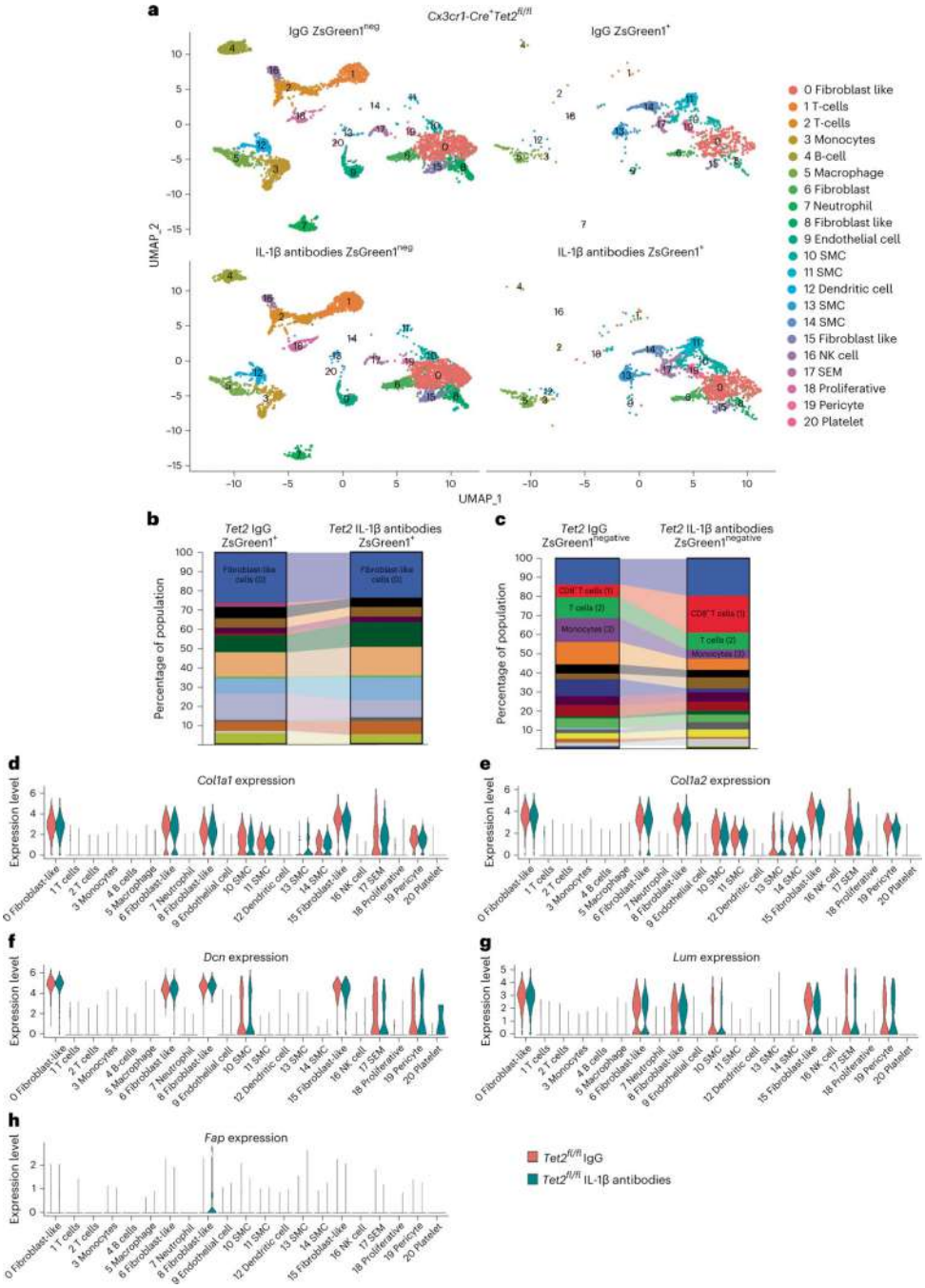

Fig. 5 |. Cluster 0 fibroblast-like cells are enriched for matrix genes in mice modeling *Tet2* CH.
a, UMAP visualization of cells isolated from aortas of mice lacking *Tet2* in monocytes and macrophages, sorted based on treatment and ZsGreen1 status (5 mice pooled together per sample). **b**,**c**, scRNA-seq population distribution of ZsGreen1^{+} Myh11-derived cells (**b**) and ZsGreen1^{Neg} cells (**c**). **d**–**h**, Violin plots of scRNA-seq data of ZsGreen1^{+} and ZsGreen1^{Neg} cells (pooled together) from mice modeling *Tet2* CH for *Col1a1* (**d**), *Col1a2* (**e**), *Dcn* (**f**), *Lum* (**g**) and *Fap* (**h**).

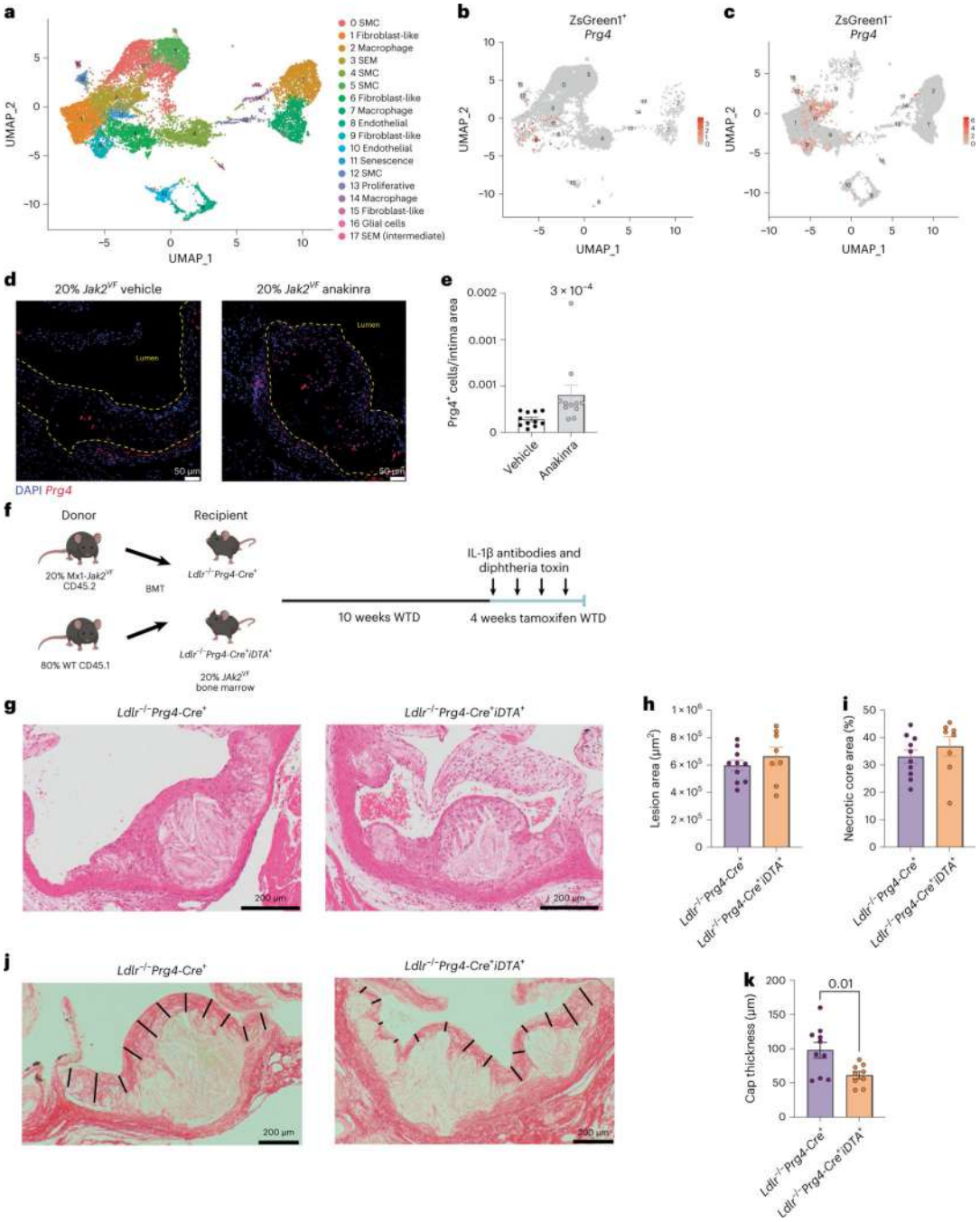

Fig. 6 |. Ablation of *Prg4*$^{+}$ cells blunts IL-1β antibody-mediated cap thickening.

a–**c**, UMAP visualization of scRNA-seq of aortas from mice modeling *Jak2* CH (**a**) (related to Fig. 2j) overlayed with *Prg4* expression in ZsGreen1^{+} (**b**) or ZsGreen1^{Neg} (**c**) cells. **d**, Representative RNAscope images of plaques, indicated with dashed yellow lines, from mice modeling *Jak2*^{VF} CH treated with anakinra for 12 weeks (n = 11). **e**, Quantification of *Prg4*$^{+}$ cells in lesions (n = 11). **f**, Experimental scheme for deletion of *Prg4*$^{+}$ cells with iDTA. **g**, Representative H&E images of aortic roots of male and female mice treated as indicated in **f** (n = 10 *Ldlr*$^{-/-}$*Prg4-Cre*$^{+}$, n = 8 *Ldlr*$^{-/-}$*Prg4-Cre*$^{+}$*iDTA*$^{+}$). **h**,**i**, Quantification

of lesion area (**h**) and percentage necrotic core area (**i**) ($n = 10$ *Ldlr*$^{-/-}$*Prg4-Cre*$^{+}$, $n = 8$ *Ldlr*$^{-/-}$*Prg4-Cre*$^{+}$*iDTA*$^{+}$). **j**, Representative picrosirius red staining of aortic root lesions; black bar indicates cap thickness ($n = 10$ *Ldlr*$^{-/-}$*Prg4-Cre*$^{+}$, $n = 9$ *Ldlr*$^{-/-}$*Prg4-Cre*$^{+}$*iDTA*$^{+}$). **k**, Quantification of cap thickness ($n = 10$ *Ldlr*$^{-/-}$*Prg4-Cre*$^{+}$, $n = 9$ *Ldlr*$^{-/-}$*Prg4-Cre*$^{+}$*iDTA*$^{+}$). Data are mean ± s.e.m. Two-tailed Student's *t*-test (**h**, **i** and **k**). Two-tailed Mann–Whitney (**e**).

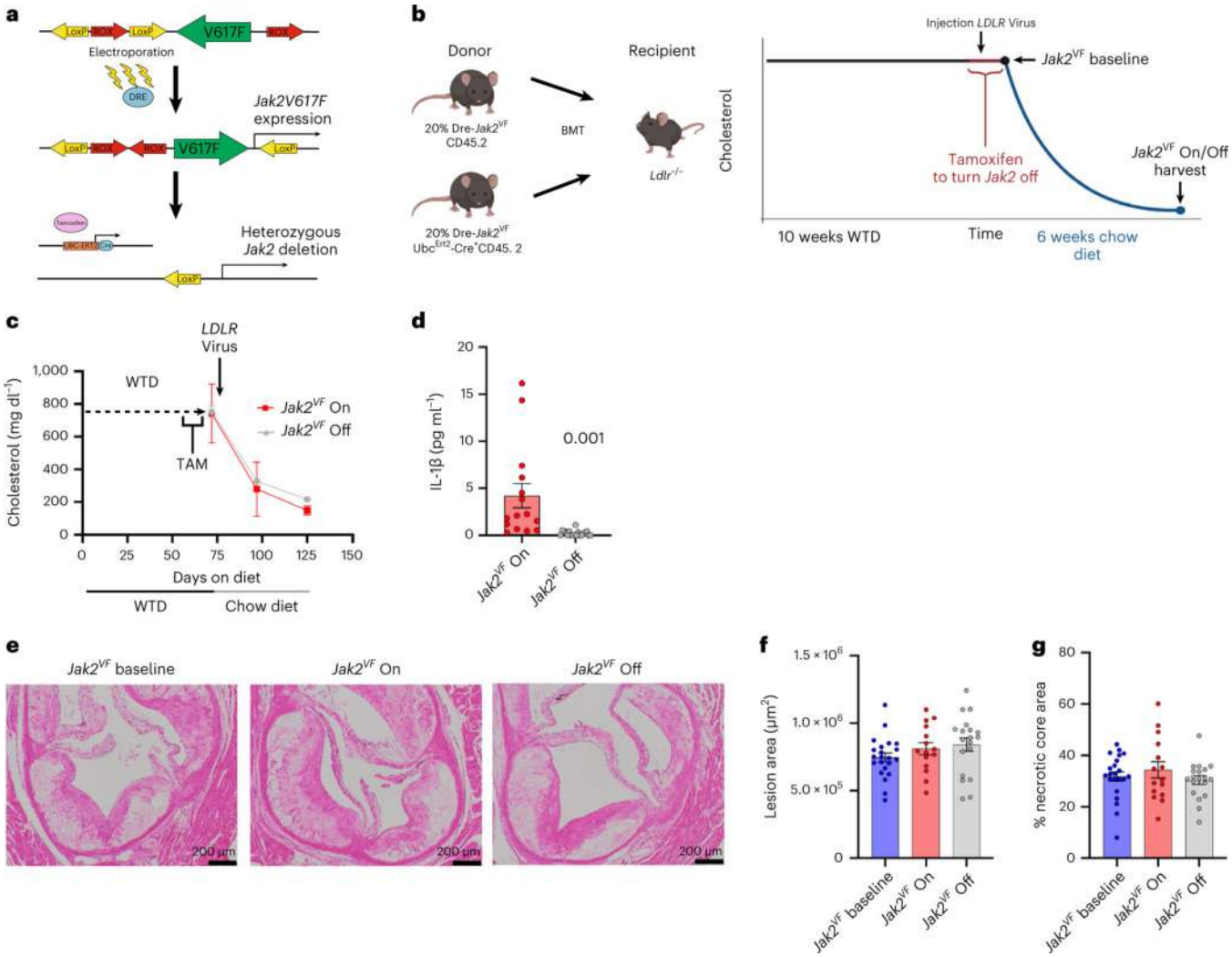

Fig. 7 |. Genetic ablation of *Jak2*^{VF} coupled to cholesterol lowering.

a, Experimental scheme of Dre-mediated *Jak2*^{VF} expression in bone marrow cells before BMT. **b**, Experimental scheme for cholesterol lowering strategy. **c**, Serum cholesterol in mice modeling *Jak2*^{VF} CH; tamoxifen (TAM) diet was administered to all mice, then a baseline group was collected. *LDLR* adenovirus (AAV) was administered with chow diet to decrease cholesterol (n = 18 *Jak2*^{VF} On, n = 16 *Jak2*^{VF} Off). **d**, IL-1β concentration in serum following cholesterol lowering (day 125) (n = 15 *Jak2*^{VF} On, n = 19 *Jak2*^{VF} Off). **e**, Representative H&E images of aortic root lesions (n = 22 control, n = 15 *Jak2*^{VF} On, n = 19 *Jak2*^{VF} Off). **f**,**g**, Quantification of aortic root lesion area (**f**) and necrotic core area (**g**) of mice treated as indicated in (n = 22 control, n = 15 *Jak2*^{VF} On, n = 19 *Jak2*^{VF} Off). Data are mean ± s.e.m. Two-way ANOVA with Tukey's multiple comparisons test (**b**). Two-tailed Student's t-test (**d**). One-way ANOVA with Tukey's multiple comparisons test (**f** and **g**).

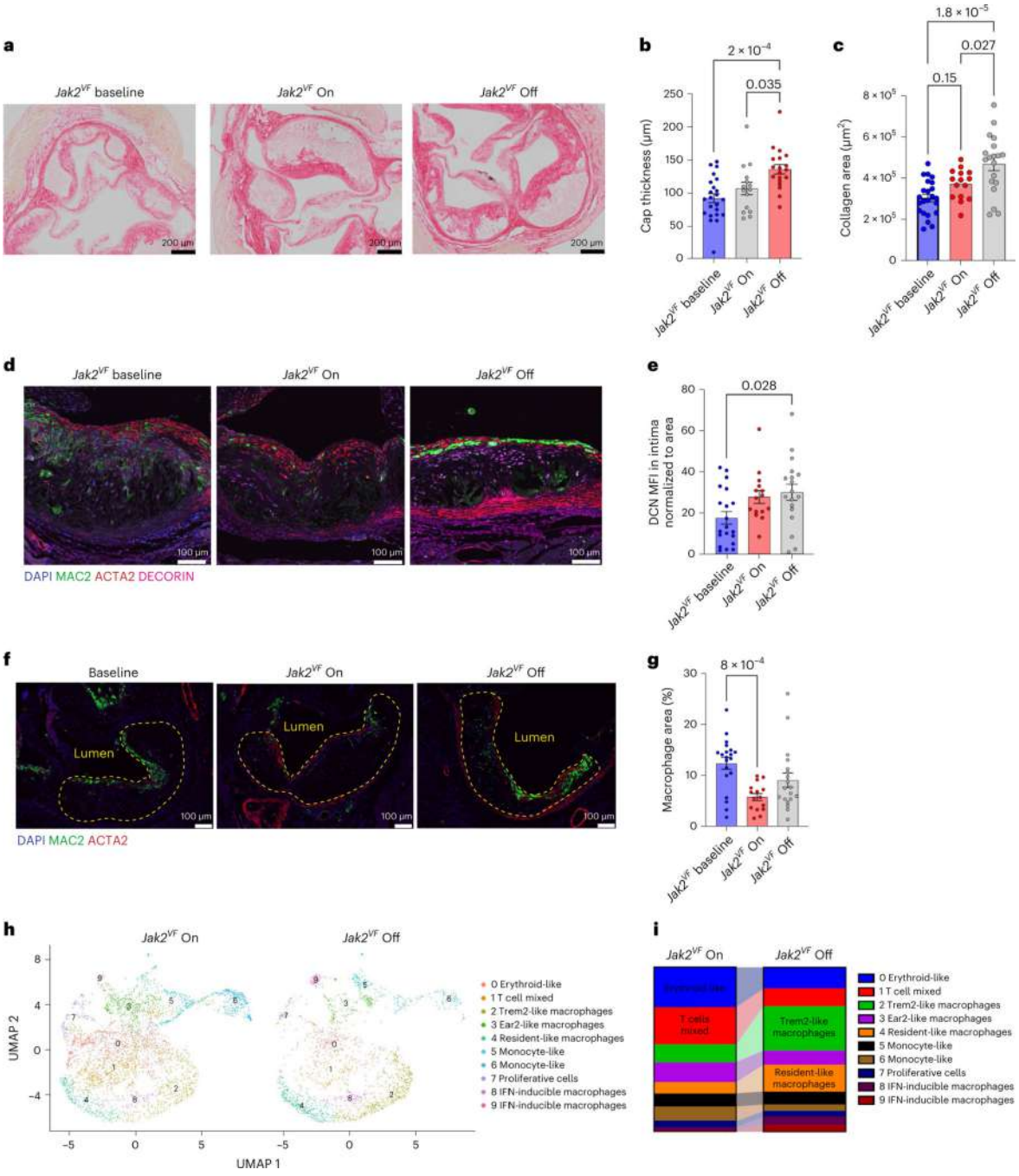

Fig. 8 |. Turning *Jak2*^{VF} off promotes cap thickening when coupled to aggressive cholesterol lowering.

a, Representative images of lesions stained with picrosirius red (n = 23 control, n = 15 *Jak2*^{VF} On, n = 19 *Jak2*^{VF} Off). **b**,**c**, Quantification of fibrous cap thickness (**b**) and collagen content in aortas (**c**) (n = 23 control, n = 15 *Jak2*^{VF} On, n = 19 *Jak2*^{VF} Off). **d**, IF staining of aortic root lesions (n = 20 control, n = 15 *Jak2*^{VF} On, n = 19 *Jak2*^{VF} Off). **e**, Quantification of Decorin expression normalized to intima area (n = 20 control, n = 15 *Jak2*^{VF} On, n = 19 *Jak2*^{VF} Off). **f**, IF staining of lesions; dashed yellow area indicates lesions (n = 20 control,

n = 15 *Jak2*^{VF} On, *n* = 19 *Jak2*^{VF} Off). **g**, Quantification of macrophage (MAC2^{+}) area in lesions (*n* = 20 control, *n* = 15 *Jak2*^{VF} On, *n* = 19 *Jak2*^{VF} Off). **h**, UMAP visualization of myeloid subsets found in CD45^{+} aortas (each sample is 5 mice pooled together). **i**, Population distribution of scRNA-seq analysis. Data are mean ± s.e.m. One-way ANOVA with Tukey's multiple comparisons test (**b** and **c**). Kruskal–Wallis test with Dunn's multiple comparisons (**e** and **g**).